KAPL-P-000083
(K98073)

CONF-9805146--

RECEIVED
JAN 19 1999
OSTI

TERNARY AND QUATERNARY ANTIMONIDE DEVICES FOR THERMOPHOTOVOLTAICS APPLICATIONS

C.W. Hitchcock, R. H. Gutmann, M. J. Freeman, G. W. Charache

June 1998

DISTRIBUTION OF THIS DOCUMENT IS UNLIMITED

MASTER

NOTICE

This report was prepared as an account of work sponsored by the United States Government. Neither the United States, nor the United States Department of Energy, nor any of their employees, nor any of their contractors, subcontractors, or their employees, makes any warranty, express or implied, or assumes any legal liability or responsibility for the accuracy, completeness or usefulness of any information, apparatus, product or process disclosed, or represents that its use would not infringe privately owned rights.

KAPL ATOMIC POWER LABORATORY SCHENECTADY, NEW YORK 12301

Operated for the U. S. Department of Energy
by KAPL, Inc. a Lockheed Martin company

DISCLAIMER

This report was prepared as an account of work sponsored by an agency of the United States Government. Neither the United States Government nor any agency thereof, nor any of their employees, makes any warranty, express or implied, or assumes any legal liability or responsibility for the accuracy, completeness, or usefulness of any information, apparatus, product, or process disclosed, or represents that its use would not infringe privately owned rights. Reference herein to any specific commercial product, process, or service by trade name, trademark, manufacturer, or otherwise does not necessarily constitute or imply its endorsement, recommendation, or favoring by the United States Government or any agency thereof. The views and opinions of authors expressed herein do not necessarily state or reflect those of the United States Government or any agency thereof.

DISCLAIMER

Portions of this document may be illegible in electronic image products. Images are produced from the best available original document.

Ternary and Quaternary Antimonide Devices for Thermophotovoltaic Applications

C.W. Hitchcock, R.J. Gutmann, H. Ehsani, I.B. Bhat
Center for Integrated Electronics and Electronics Manufacturing
Rensselaer Polytechnic Institute, Troy, NY 12180-3590

C.A. Wang
Lincoln Laboratory, Massachusetts Institute of Technology

M.J. Freeman and G.W. Charache
Lockheed Martin, Inc., Schenectady, NY 12301

Abstract

Thermophotovoltaic (TPV) devices have been fabricated using epitaxial ternary and quaternary layers grown on GaSb substrates. GaInSb ternary devices were grown by metalorganic vapor phase epitaxy (MOVPE) with buffer layers to accommodate the lattice mismatch, and GaInAsSb lattice-matched quaternaries were grown by MOVPE and by liquid phase epitaxy (LPE). Improved devices are obtained when optical absorption occurs in the p-layer due to the longer minority carrier diffusion length. Thick emitter p/n devices are limited by surface recombination, with highest quantum efficiency and lowest dark current being achieved with epitaxially grown surface passivation layers on lattice-matched MOVPE quaternaries. Thin emitter/thick base n/p devices are very promising, but require improved shallow high-quality n-type ohmic contacts.

1 Introduction

Thermophotovoltaic (TPV) devices are being explored for a variety of terrestrial and space applications [1–4]. The systems approach has been to use silicon devices matched to selective emitters or design low-band gap compound semiconductor cells matched to blackbody emitters. This paper presents results of epitaxial devices on GaSb substrates for TPV applications requiring band gap energies near 0.55 eV, focusing on electrical parameters achieved with different epitaxial growth techniques and alternative device structures.

2 Device Structures and Epitaxial Techniques

In order to maximize both the efficiency and the power density of TPV devices, we examined device structures which minimize saturation current density, allowing devices to be operated at high forward bias without significant dark current loss, while maintaining high collection efficiency of photogenerated carriers. The material properties required to achieve these device goals are maximum minority carrier diffusion length, minimum minority carrier recombination at device surfaces, and optimum device doping profiles. The generic device structure is shown in figure 1, with the key parameters of 9 device types presented in table 1.

In order to achieve the required characteristics, we considered four different device structures. The first structure consists of a thin p-type emitter and a thick n-type base (device type 1). The majority of the photon absorption occurs in the n-type base; therefore, the hole diffusion length in the base and the base back surface recombination velocity are of critical importance. The high doping required to minimize series resistance, along with the close proximity of the front surface, produces high minority carrier losses, and the efficiency associated with the emitter is low. In our experience, obtaining a suitably large minority carrier diffusion length in the n-type base has been a problem due to: (1) the relatively low hole mobility in this region, (2) the potential for deep level defects associated with the Te dopant [5], and (3) higher Auger recombination rates in n-type material [6].

The second device structure, considered in-depth, is the thick p-emitter, thin n-base configuration (device types 2–8). Here all of the absorption takes place in the emitter, so the minority carrier properties of the base are important only for reducing the dark current. The large width of the emitter allows a reasonably low doping without introducing excessive series resistance, and the large minority electron mobility in the absorption region is an advantage. The principal disadvantage is that most of the absorption takes place close to the device front surface. Unless the front surface is a very good minority carrier mirror, surface losses will dominate. In order to achieve a better minority carrier mirror, several surface passivations have been attempted by growing epitaxial layers of larger bandgap on the front surface (device types 5–8).

The third device structure is the thin n-emitter, thick p-base configuration (device type 9). Here, losses due to absorption in the heavily doped, surface n-emitter will still be present, but the emitter can be shallower and/or less heavily doped due to the higher mobility of the majority electrons in the

lateral current flow to the front contact. In the p-type base, efficient minority carrier transport to the collection junction can occur without the losses due to a poor surface. The principal disadvantage of this device design is the difficulty associated with contacting a thin n-type layer. The anneal required for ohmic contacts to n-type material generally produces a reaction which extends through the emitter and short circuits the device junction.

The fourth device structure, described for completeness, is the thick n-emitter, thin p-base arrangement. The thicker emitter can help alleviate some of the front contact difficulties, but at the expense of introducing a large n-type absorbing region, which is inefficient due to both the low minority carrier diffusion length and the poor front surface.

The ternary ($In_{0.2}Ga_{0.8}Sb$) device layers (device types 1,2,6,8,9) were grown by metalorganic vapor phase epitaxy (MOVPE) on (100) oriented GaSb substrates in a low pressure, rf-heated, horizontal MOVPE reactor [2]. Trimethylgallium, trimethylindium, trimethylantimony, silane, and diethyltellurium were used as the Ga, In, Sb, Si, and Te sources, respectively. After degreasing the wafers in organic solvents, the GaSb wafers were etched in a 1% bromine-methanol solution for 30 seconds immediately prior to loading in the growth chamber. An initial layer of heavily doped n-type GaSb was grown on the substrate surface to a thickness of approximately 300nm, and then the group III composition was stepped to 20% indium over the course of approximately a micron of growth. Base and emitter layers of $Ga_{0.8}In_{0.2}Sb$ were grown with varying thicknesses and dopings. The growth temperature was in the range from 580°C to 600°C, with resultant growth rates of 1.8 to 2.4μm/hr.

The quaternary ($Ga_{0.87}In_{0.13}As_{0.12}Sb_{0.88}$) device layers (device types 3,5,7) were grown by MOVPE on (100) Te-doped GaSb substrates misoriented 6° toward (111)B [3]. A vertical rotating-disk reactor with H_2 carrier gas at a flow rate of 10 slpm and a pressure of 150 Torr was used. Organometallic sources included trimethylindium, triethylgallium, tertiarybutylarsine, and trimethylantimony, and n and p dopant sources were diethyltellurium (50 ppm in H_2) and dimethylzinc (1000ppm in H_2), respectively. The growth temperature ranged from 525°C to 575°C, and the growth rate was approximately 2.7 μm/hr.

The quaternary $Ga_{1-x}In_xAs_ySb_{1-y}$ epitaxial device layers (device type 4) were grown by liquid phase epitaxy (LPE) lattice matched to nominal (100) Te-doped GaSb substrates. A conventional horizontal graphite source-seed sliding boat in a Pd-diffused hydrogen atmosphere was used. Following

preparation of the constituent components and substrate cleaning, the solution was remelted at 560°C for 1 hour followed by a slow temperature ramp to the liquidus temperature of 532°C. A growth temperature of 530°C (2°C supersaturation) was chosen to avoid homogeneous nucleation, with a resulting growth rate of approximately 0.5μm/min. Layers were shiny and reflective with small solution puddles.

3 Device Fabrication Techniques

In order to produce TPV devices, conventional semiconductor processing techniques were employed. Initially, the samples were cleaned using acetone, methanol, and isopropanol to remove organic contaminants, followed by a brief immersion in 20:1 hydroflouric acid to remove surface oxide. Immediately following the HF immersion, the samples were placed under vacuum and a blanket contact metal was applied to the sample back surface by e-beam evaporation. Devices with n-type substrates underwent an anneal after back contact formation. Next photoresist was applied to the front of the sample and patterned using a complex liftoff process described elsewhere [4]. After the photoresist was developed (exposing the areas to be contacted) the samples were cleaned with a 20:1 HF immersion and placed immediately under vacuum. The front grid metal was deposited by e-beam evaporation, followed by completion of the liftoff process. The devices then underwent another photolithography process to isolate the nominally 1 cm^2 cells; the active areas were protected with a thin layer of photoresist and the emitter epilayers outside the active region were etched away in an $HCl : H_2O_2$: NaK Tartrate solution (66mL:18mL:24g in 1L of solution).

For p-type contacts, 200nm of gold were deposited and then capped with 1 to 2 microns of silver. The gold layer was chosen to produce a good interface while the silver layer provided low resistivity bulk and a good surface for probing. No contact anneal was required for p-type contacts, as the Fermi level is pinned near the valence band of these semiconductors, regardless of the work function of the contact metal [7], so that contacts to p-type materials are generally ohmic as deposited and produce specific contact resistances between 10^{-4} and $10^{-5}\,\Omega cm^2$ as measured by the method of Cox and Strack [8,9]. While lower specific contact resistances have been obtained with other surface cleans and post-deposition anneals [10], $10^{-4}\,\Omega cm^2$ has only a minor effect on contact grid design.

For n-type contacts to bulk materials, an evaporation of 10nm tin followed by 200nm of gold was employed [11], with the unalloyed contact being non-ohmic. The devices were alloyed at 350°C for 5 seconds, with a resultant specific contact resistance between 10^{-4} and $10^{-5}\,\Omega\text{cm}^2$.

The contacting method used for bulk n-type layers has not been successful for shallow n-type contacts. During the anneal, a reaction occurs between the gold, tin, and semiconductor. The gold surface turns silvery gray during the anneal. Electrically, p-n diodes with thin n-type emitters contacted with the bulk-n metallization become short circuits during the anneal. Physically, a reaction occurs between the metals and the semiconductor material so that all of the n-type layer is consumed in some places, and the metal contacts the p-type layer below.

A nonshorting contact to a thin n-type emitter requires a reduced reaction between the metal and the semiconductor. A titanium layer at least 50nm thick inhibits such a reaction, so that other metals can be deposited subsequently without affecting the titanium semiconductor junction. Initial results with a structure of 10 nm of tin followed by 150nm of titanium, 50nm of gold, and $1 - 2\,\mu$m of silver annealed at 350°C for $5s$ produced functional but leaky devices.

4 Characterization Techniques

In order to determine the underlying physics of the semiconductor junctions, I-V and quantum efficiency characteristics were measured. Due to the high current, low voltage nature of thermophotovoltaic devices, Kelvin contacting methods were used for both front and rear contacts.

Room temperature dark I-V measurements taken in both the forward and reverse directions agreed with the expected device behavior using the following relationship:

$$I = I_s \cdot \left[exp\left(\frac{q\,(V - I \cdot R_e)}{nkT} \right) - 1 \right] + \frac{V - I \cdot R_e}{R_u} \tag{1}$$

where I represents device current, I_s represents saturation current, V represents the applied voltage, n is an ideality factor that is expected to be between 1 and 2 for various regions of device operation, R_e is the series resistance, R_u is the shunt resistance, and kT is the thermal energy.

In addition, devices were also measured under high illumination conditions. The simplest model of a TPV device under optical illumination is described by equation (1) with $R_e = 0$, R_u infinite, and a current source corresponding to carrier generation in parallel with the entire device, leading to the device model:

$$I = I_s \cdot \left[exp\left(\frac{qV}{nkT}\right) - 1\right] - I_L \tag{2}$$

where I_L is the magnitude of the light generation current. A more intricate model with parasitic resistances is more complicated, but this simple model is usually adequate.

Quantum efficiency measurements differ from illuminated measurements under TPV conditions in three principal respects. First, quantum efficiency measurements occur under monochromatic illumination, with the photoresponse of the test junction measured at one particular wavelength. Second, standard quantum efficiency measurements occur at much lower levels of illumination than TPV operating conditions. Third, quantum efficiency measurements are not taken with the device biased at the maximum power point of its I-V characteristic or along a range of bias points, but only at the zero voltage (short circuit) bias point.

Since the material absorption coefficient of GaSb is known reasonably well as a function of wavelength [12,13] and the absorption coefficients of related ternaries and quarternaries can be estimated with reasonable accuracy [14]; a theoretical quantum efficiency curve can be simulated for a device with known emitter and base thicknesses and assumed minority carrier diffusion lengths and surface recombination velocities. The theoretical curve can be compared to the empirical curve, and the unknown parameters (diffusion lengths and surface recombination velocities) can be adjusted to produce a fit. The curve fit obtained is generally unique and a reasonable value of the unknown parameters can be extracted (or in some cases a lower or upper bound).

5 Results and Discussion

This study focused on thick p-emitter thin n-base structures, unlike earlier generations of devices described previously [4]. For these structures, we fabricated devices on three different families of epitaxial material described in section 2.

Figures 2, 3, and 4 illustrate external quantum efficiencies of device types 2, 3, and 4 respectively — some of the best unpassivated devices of each family. In figures 2 and 3 the experimental curves are presented along with theoretical curves fit to the data. Diffusion lengths and surface recombination velocities can be deduced from these fits, although obtaining unique parameter values may not be possible in all cases. For example, figure 2 presents a device with a very lossy emitter. Although the slope of the curve allows us to state that most of the loss is at the front surface of the emitter, a finite bulk recombination component could be present but masked by the large surface loss. We present a lower bound for the corresponding bulk diffusion length.

Comparing figures 2, 3, and 4, in each case the efficiency peaks near 2150 nm, decreasing rapidly at longer wavelengths and more gradually at shorter wavelengths. The lack of collection at longer wavelengths indicates that all three devices have a bandgap of approximately 0.57eV, while the slower but still pronounced decrease at shorter wavelengths is indicative of a poor front surface. Since shorter wavelength photons have higher absorption coefficients, they are absorbed more predominantly near the front surface, and the poor surface reduces collection efficiency. Note that the quantum efficiencies for all three devices are nearly identical.

Figure 5 illustrates quantum efficiencies for devices identical in all respects to those of figure 3 except that (1) in device type 5, the emitter has been capped with a GaSb window and (2) in device type 7, the emitter has been capped with a quaternary AlGaAsSb window as well as a GaSb window. In both cases, the addition of an effective minority carrier mirror results in a considerable improvement in external quantum efficiency, with the characteristics peaking at 40 to 45 percent and remaining more constant from 1200nm to 2100nm. Also shown in figure 5 is the quantum efficiency of a ternary epilayer device with a highly doped ternary epilayer window layer (device type 8). While there is some modest improvement in the device characteristic, a dramatic improvement in quantum efficiency that occurred for the quaternary is not obtained. However, the dark current density for this device has been reduced significantly (as discussed subsequently).

While the quantum efficiency curves illustrate the relative collection efficiencies of the devices at various wavelengths, they fail to provide information concerning device performance under realistic high-intensity illumination. Figure 6 displays short circuit current density versus open circuit voltage for several p-emitter devices. Improvements in minority carrier diffu-

sion length will move a device curve toward the right, achieving a higher open circuit voltage for a given short circuit current and higher overall device efficiency. Curves A and B are an initial thick p-emitter ternary epilayer device (device type 8) and a quaternary with excellent surface passivation (device type 7), respectively. For this high optical intensity characterization, these two samples are the worst and best cases respectively; they also comprise a convenient baseline to which to compare other devices. The dark saturation current density for the baseline curves, ranging from a high of $0.1\,mA/cm^2$ to a low of $0.005\,mA/cm^2$ are included in figure 6. The remaining curves of figure 6 trace the recent history of device development for the thick p-emitter family of devices.

Figure 7 represents the best device in the thin p-emitter thick base family (device type 1). The shape of the quantum efficiency curve is much different from the unpassivated thick-p emitter curves, peaking at a higher value and at shorter wavelengths. The peak value is still lower than those of the passivated curves of figure 5. Additionally, note that the efficiencies of the passivated curves fall off less in the near-bandgap region.

Figure 8 is a quantum efficiency measurement of the best example of device type 9. The emitter thickness of $0.9\,\mu$m is larger than desired in order to allow processing of the front contact without damaging the junction. Figure 9 indicates that the high current illuminated characteristics of this device are quite good; this unpassivated ternary device with lattice mismatched active layers is approaching the performance of quaternary devices with AlGaAsSb passivation layers and a completely lattice-matched structure.

6 Summary

The two most promising device structure for antimonide-based TPV devices are either thick p-emitter, n-base devices with well passivated front surfaces (minority carrier mirrors to reduce the effective surface recombination velocity) or thin n-emitter, thick p-base devices with non-shorting ohmic contacts. For quaternary epitaxial layers lattice-matched to GaSb substrates, the former structure is presently preferred as lattice-matched capping layers of AlGaAsSb can be readily grown. For ternary epitaxial layers, effective capping with epitaxial layers has not been developed, and the thin n-emitter thick p-base structure is preferred (even though shallow ohmic contacts are not fully developed). Optical absorption in p-type layers is strongly preferred

because of the longer electron diffusion length in these materials.

Two key performance metrics have been used in this work, namely quantum efficiency and dark (saturation) current. Both high quantum efficiency and low dark current are needed to achieve maximum TPV device performance (i.e., high electrical power density and high optical-to-electrical conversion efficiency). The quantum efficiency combined with a curve of short-circuit current versus open-circuit voltage (obtained with different optical intensities) provides the relevant information for TPV cells.

These antimonide TPV cell technologies should provide power densities in the watt/cm^2 range with reasonable conversion efficiency and be attractive for TPV system applications.

References

[1] H. Ehsani, I. Bhat, C. Hitchcock, J. Borrego, and R. Gutmann. "Characteristics of GaSb and GaInSb Layers Grown by Metalorganic Vapor Phase Epitaxy". *Second NREL Conference on Thermophotovoltaic Generation of Electricity*, pages 423–433, 1995.

[2] H. Ehsani, I. Bhat, C. Hitchcock, and R. Gutmann. "Growth and Characterization of $In_{0.2}Ga_{0.8}Sb$ Device Structures Using Metalorganic Vapor Phase Epitaxy". *Third NREL Conference on Thermophotovoltaic Generation of Electricity*, pages 65–74, 1997.

[3] C. Wang, H. Choi, G. Turner, D. Spears, and M. Manfra. "Lattice-Matched Epitaxial GaInAsSb/GaSb Thermophotovoltaic Devices". *Third NREL Conference on Thermophotovoltaic Generation of Electricity*, pages 75–87, 1997.

[4] C. Hitchcock, R. Gutmann, J. Borrego, H. Ehsani, I. Bhat, M. Freeman, and G. Charache. "GaInSb and GaInAsSb Thermophotovoltaic Device Fabrication and Characterization". *Third NREL Conference on Thermophotovoltaic Generation of Electricity*, pages 89–103, 1997.

[5] J. Doerschel and U. Geissler. "Characterization of extended defects in highly Te-doped ⟨111⟩ GaSb single crystals grown by the czochralski technique". *Journal of Crystal Growth*, 121:789–789, 1992.

[6] G. Benz and R. Conradt. "Auger recombination in GaAs and GaSb". *Physical Review B*, 16(2):843–855, July 1977.

[7] J. McCaldin, T. McGill, and C. Mead. "Schottky Barriers on Compound Semiconductors: The Role of the Anion". *Journal of Vacuum Science and Technology*, 13(4):802–806, July/August 1976.

[8] R. H. Cox and H. Strack. "Ohmic Contacts for GaAs Devices". *Solid-State Electronics*, 10:1213–1218, 1967.

[9] G. P. Carver, J. J. Kopanski, D. B. Novotny, and R. A. Forman. "Specific Contact Resistivity of Metal-Semiconductor Contacts—A New, Accurate Method Linked to Spreading Resistance". *IEEE Transactions on Electron Devices*, 35(4):489–496, April 1988.

[10] B. Tadayon, C. S. Kyono, M. Fatemi, S. Tadayon, and J. A. Mittereder. "Extremely low specific contact resistivities for p-type GaSb, grown by molecular beam epitaxy". *Journal of Vacuum Science and Technology B*, 13(1):1–3, January/February 1995.

[11] C. H. Heinz. "Ohmic Contacts to p- and n-Type GaSb". *International Journal of Electronics*, 54(2):247–254, 1983.

[12] D. E. Aspnes and A. A. Studna. "Dielectric functions and optical parameters of Si, Ge, GaP, GaAs, GaSb, InP, InAs, and InSb from 1.5 to 6.0 eV". *Physical Review B*, 27(2):985–1009, January 1983.

[13] R. K. Willardson and A. C. Beer, editors. *Semiconductors and Semimetals*, volume 3. Academic Press, 1966.

[14] M. J. Zierak. *Characterization and modeling of InGaAs and InGaSb thermophotovoltaic cells and materials.* PhD thesis, Rensselaer Polytechnic Institute, 1997.

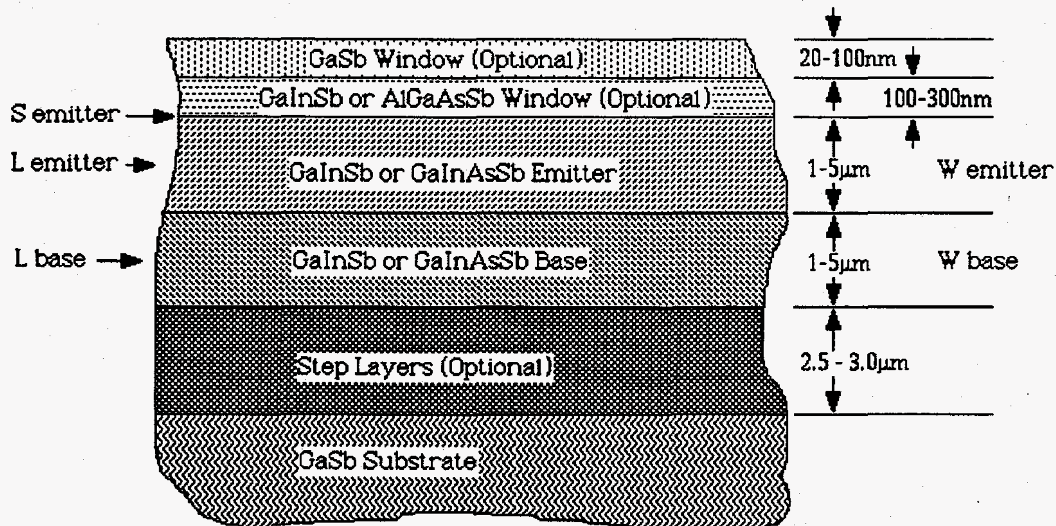

Figure 1: Generic TPV device structure. Critical parameters are W emitter, W base, S emitter (surface recombination velocity at the emitter top surface), L emitter, and L base (diffusion lengths in emitter and base)

device type	active layers	emitter type	emitter thickness (W emitter)	base thickness (W base)	window	growth technique
1	GaInSb	thin p	0.3 μm	4.5 μm	none	MOVPE
2	GaInSb	thick p	3 μm	3 μm	none	MOVPE
3	GaInAsSb	thick p	3 μm	1 μm	none	MOVPE
4	GaInAsSb	thick p	4 μm	2 μm	none	LPE
5	GaInAsSb	thick p	3 μm	1 μm	GaSb	MOVPE
6	GaInSb	thick p	4.5 μm	1 μm	GaSb	MOVPE
7	GaInAsSb	thick p	3 μm	1 μm	AlGaAsSb	MOVPE
8	GaInSb	thick p	4 μm	1.2 μm	GaInSb	MOVPE
9	GaInSb	n	0.9 μm	5 μm	none	MOVPE

Table 1: TPV device structre parameters

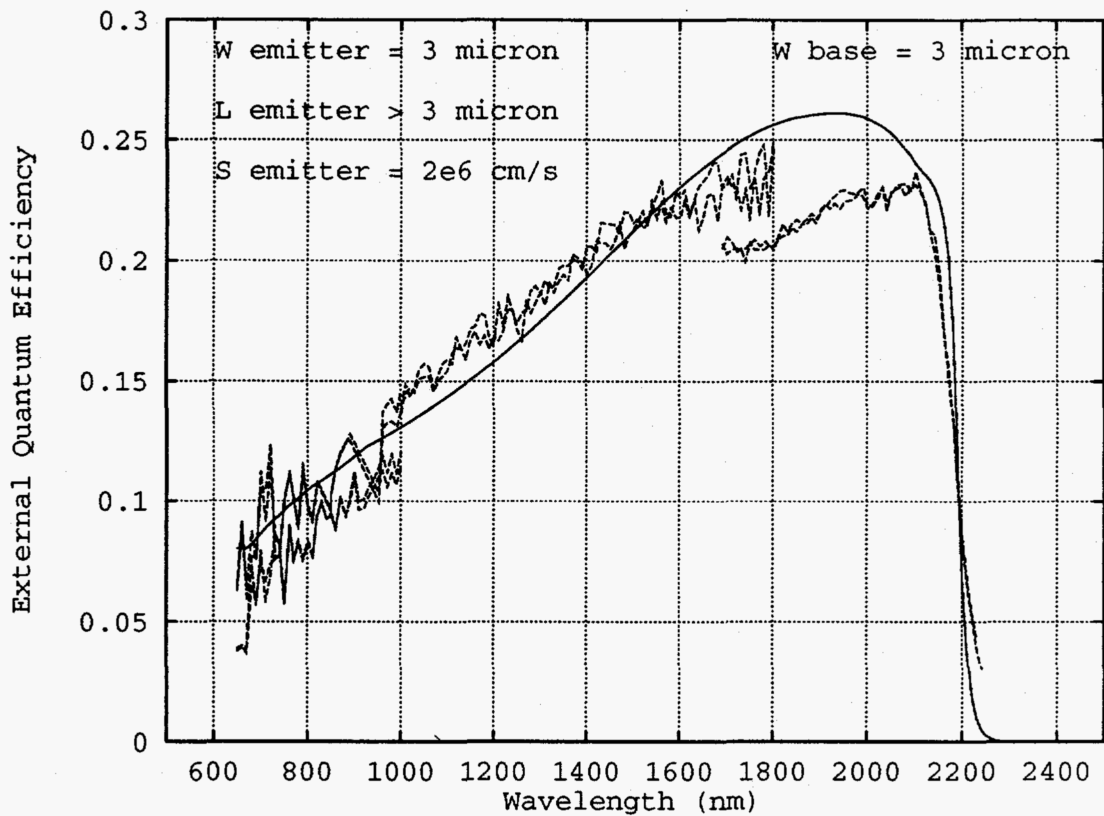

Figure 2: Thick p-emitter ternary device, no passivation (device type 2)

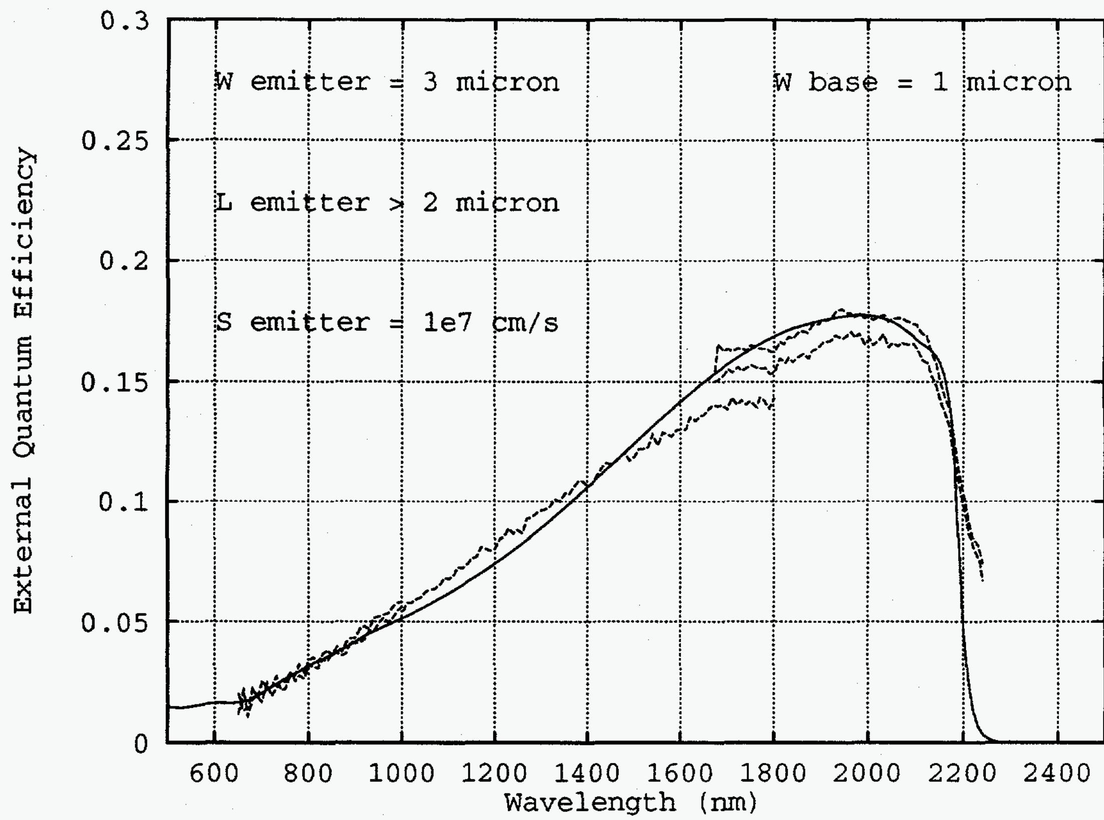

Figure 3: Thick p-emitter quaternary device, no passivation (device type 3)

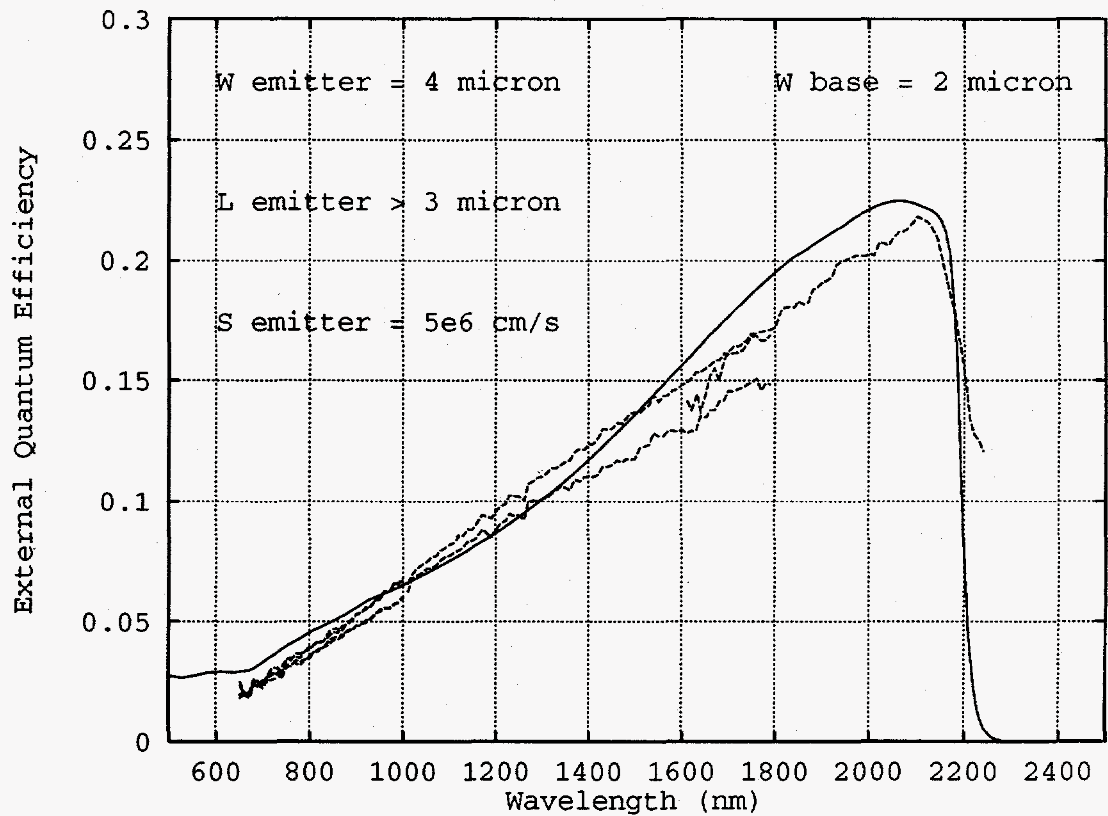

Figure 4: Thick p-emitter quaternary device, no passivation (device type 4)

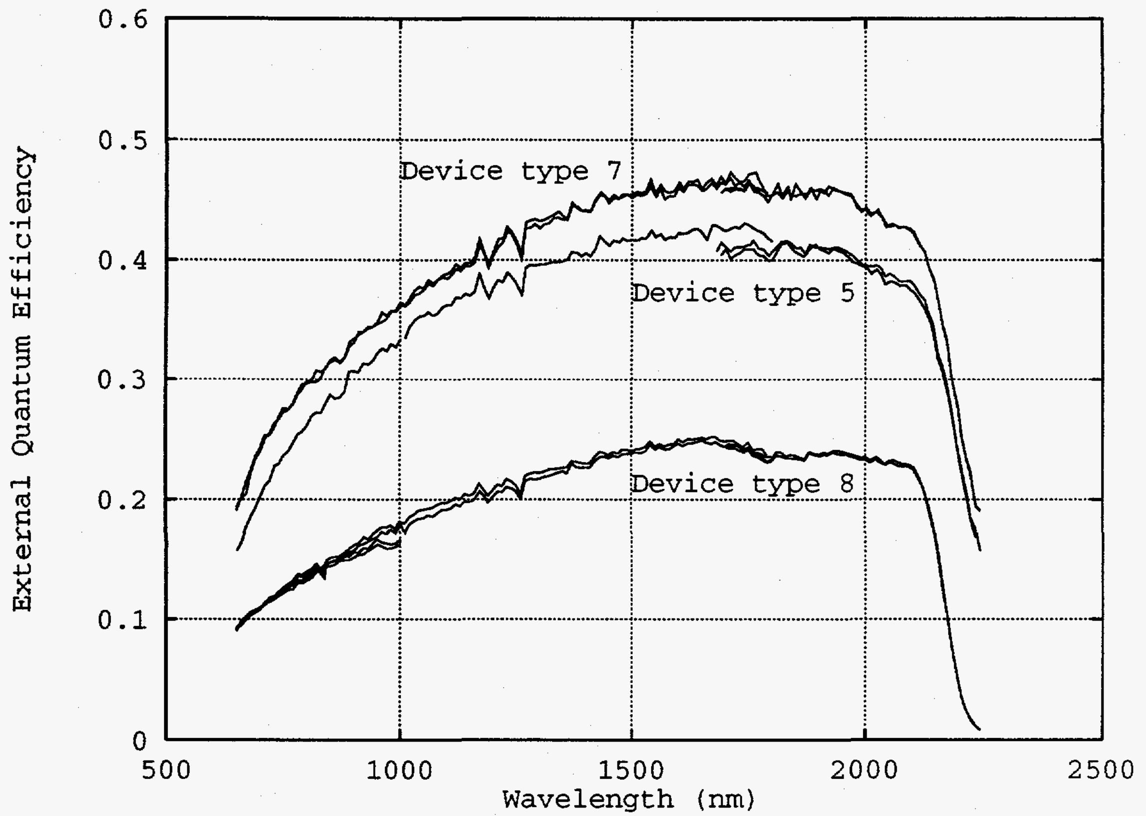

Figure 5: External quantum efficiency of passivated devices

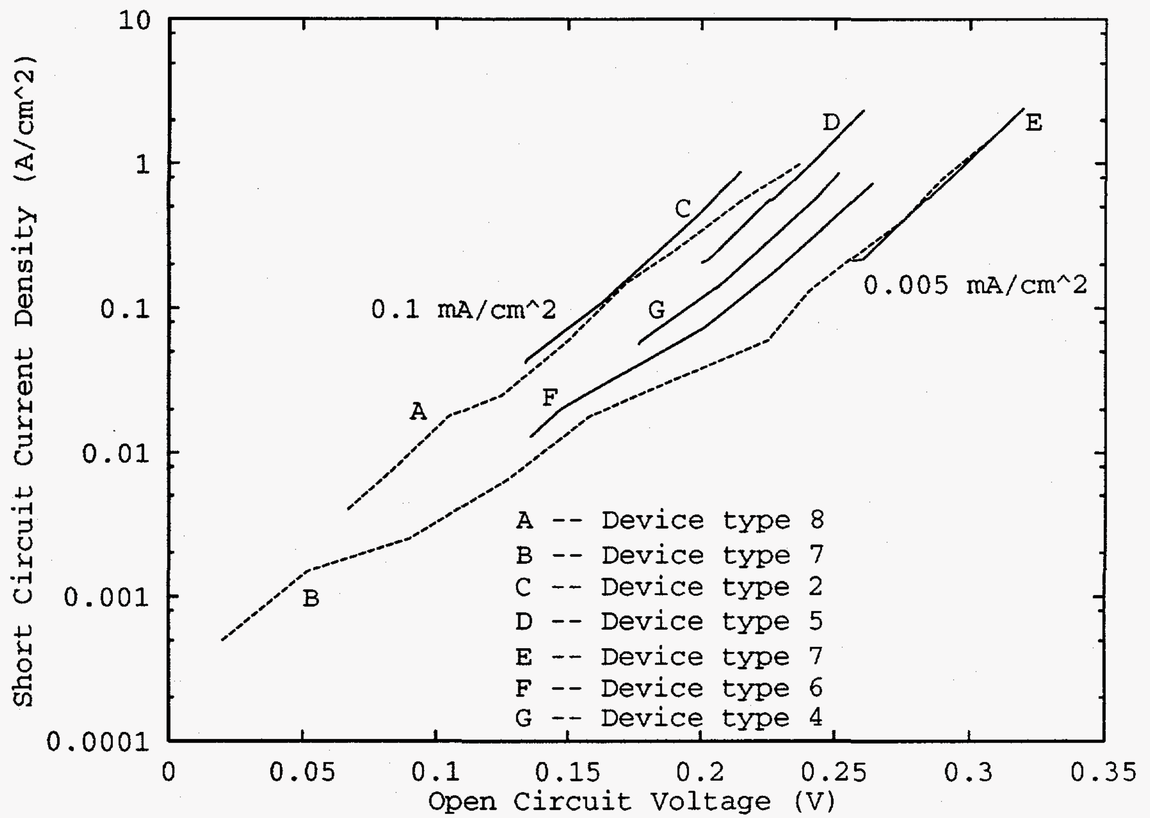

Figure 6: High Intensity Illumination Characteristics (Device type 7 was fabricated and characterized twice independently to verify performance characteristics)

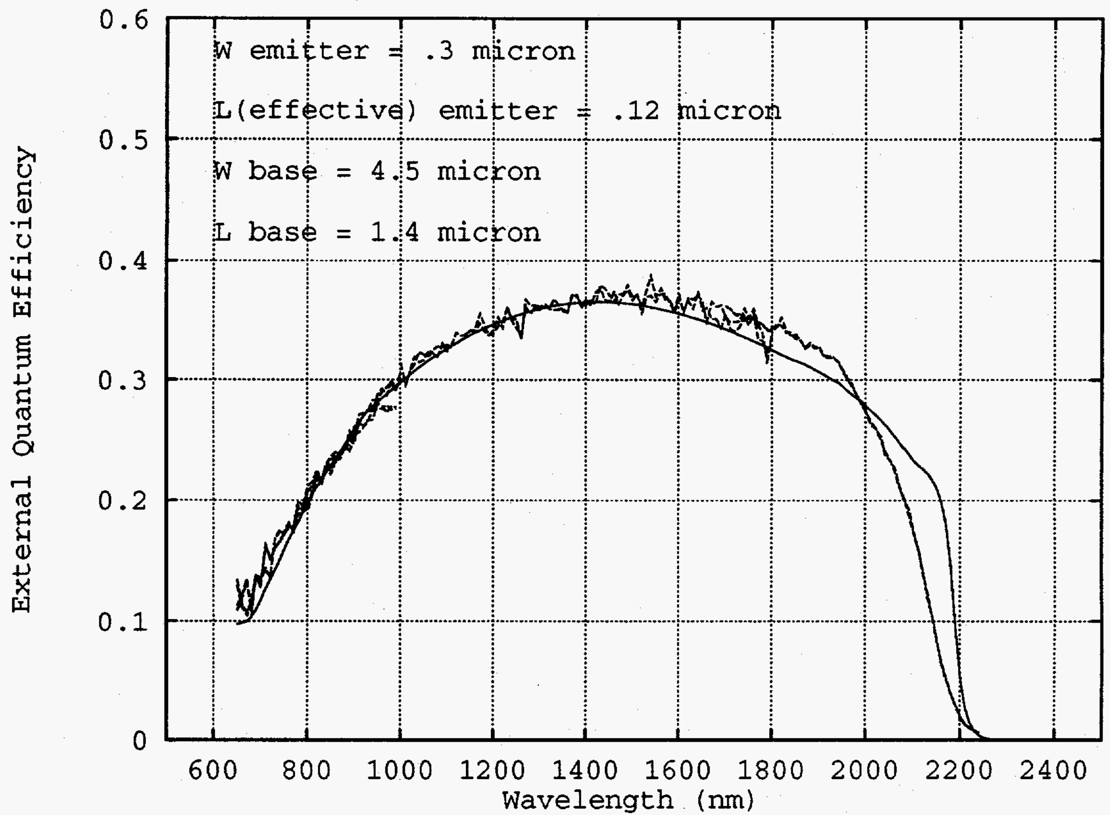

Figure 7: Thin p-emitter ternary device, no passivation (device type 1)

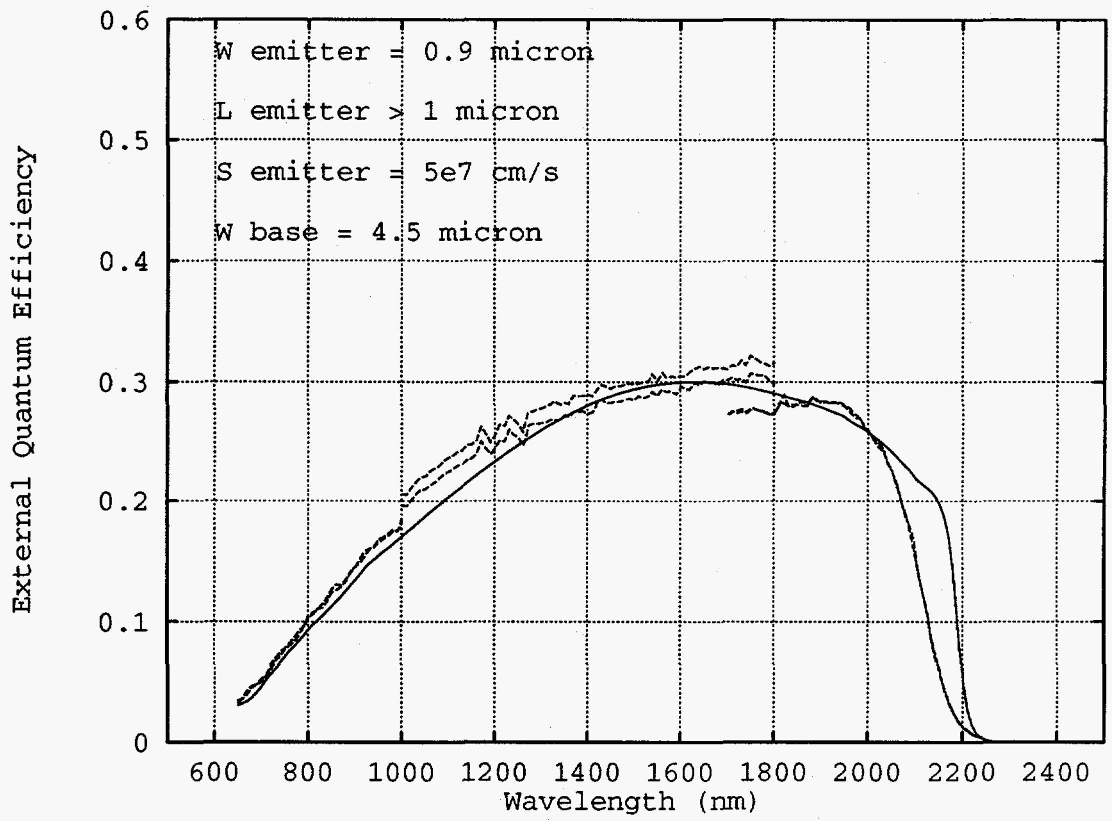

Figure 8: N-emitter device, no passivation (device type 9)

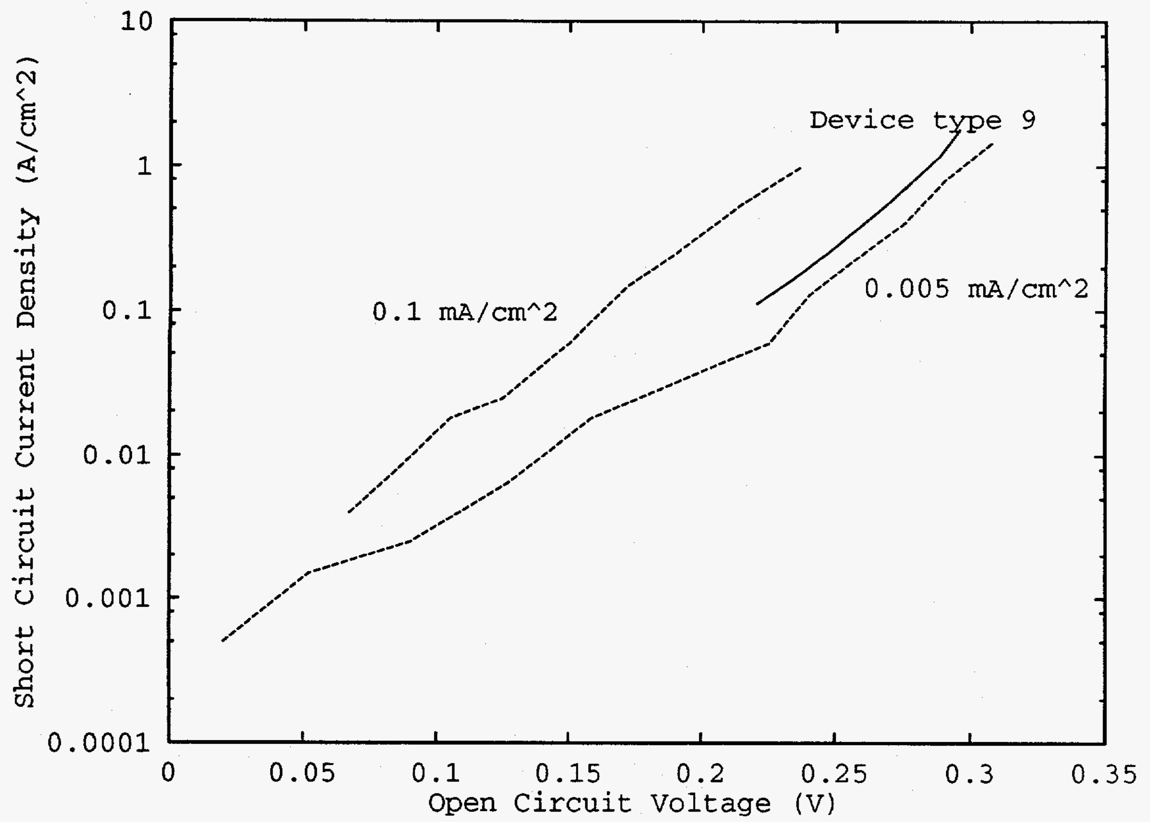

Figure 9: N-emitter device, no passivation (device type 9)

Ternary and Quaternary Antimonide Devices for Thermophotovoltaic Applications

C.W. Hitchcock, R.J. Gutmann, H. Ehsani, I.B. Bhat
Center for Integrated Electronics
and Electronics Manufacturing
Rensselaer Polytechnic Institute, Troy, NY 12180-3590

C.A. Wang
Lincoln Laboratory, Massachusetts Institute of Technology

M.J. Freeman and G.W. Charache
Lockheed Martin, Inc., Schenectady, NY 12301

ICMOVPE IX
June 1998

Outline

- Focus of program
- Device structures
- Epitaxial growth techniques
- Characterization techniques
- Device results
- Summary and conclusions

Focus of Program

- Fabricate and evaluate alternative epitaxial device structures for antimonide-based TPV cells with $E_g = 0.55$ eV;

- Delineate advantages and disadvantages of alternative structures to guide further device research;

- Delineate unit process research needs to enable further development of high-performance low-cost TPV cells.

TPV Device Structure Parameters

device type	active layers	emitter type	emitter thickness	base thickness	window	growth technique
1	GaInSb	thin p	0.3 μm	4.5 μm	none	MOVPE
2	GaInSb	thick p	3 μm	3 μm	none	MOVPE
3	GaInAsSb	thick p	3 μm	1 μm	none	MOVPE
4	GaInAsSb	thick p	4 μm	2 μm	none	LPE
5	GaInAsSb	thick p	3 μm	1 μm	GaSb	MOVPE
6	GaInSb	thick p	4.5 μm	1 μm	GaSb	MOVPE
7	GaInSb	thick p	4 μm	1 μm	GaSb	MOVPE
8	GaInAsSb	thick p	3 μm	1 μm	AlGaAsSb	MOVPE
9	GaInSb	thick p	4 μm	1.2 μm	GaInSb	MOVPE
10	GaInSb	n	0.9 μm	5 μm	none	MOVPE

Thick P-Emitter Ternary Device, No Passivation (device type 2)

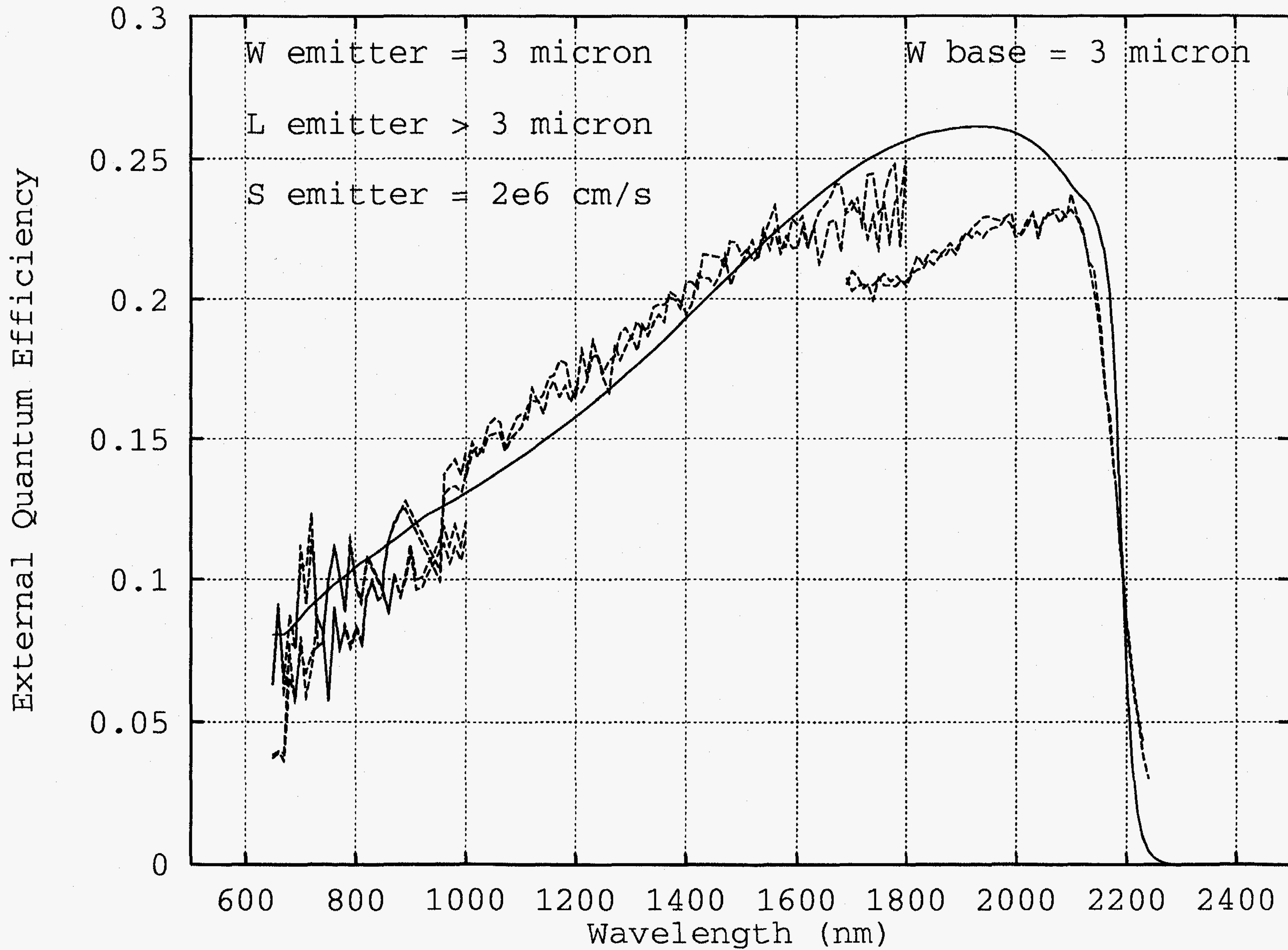

Thick P-Emitter Quaternary Device, No Passivation (device type 3)

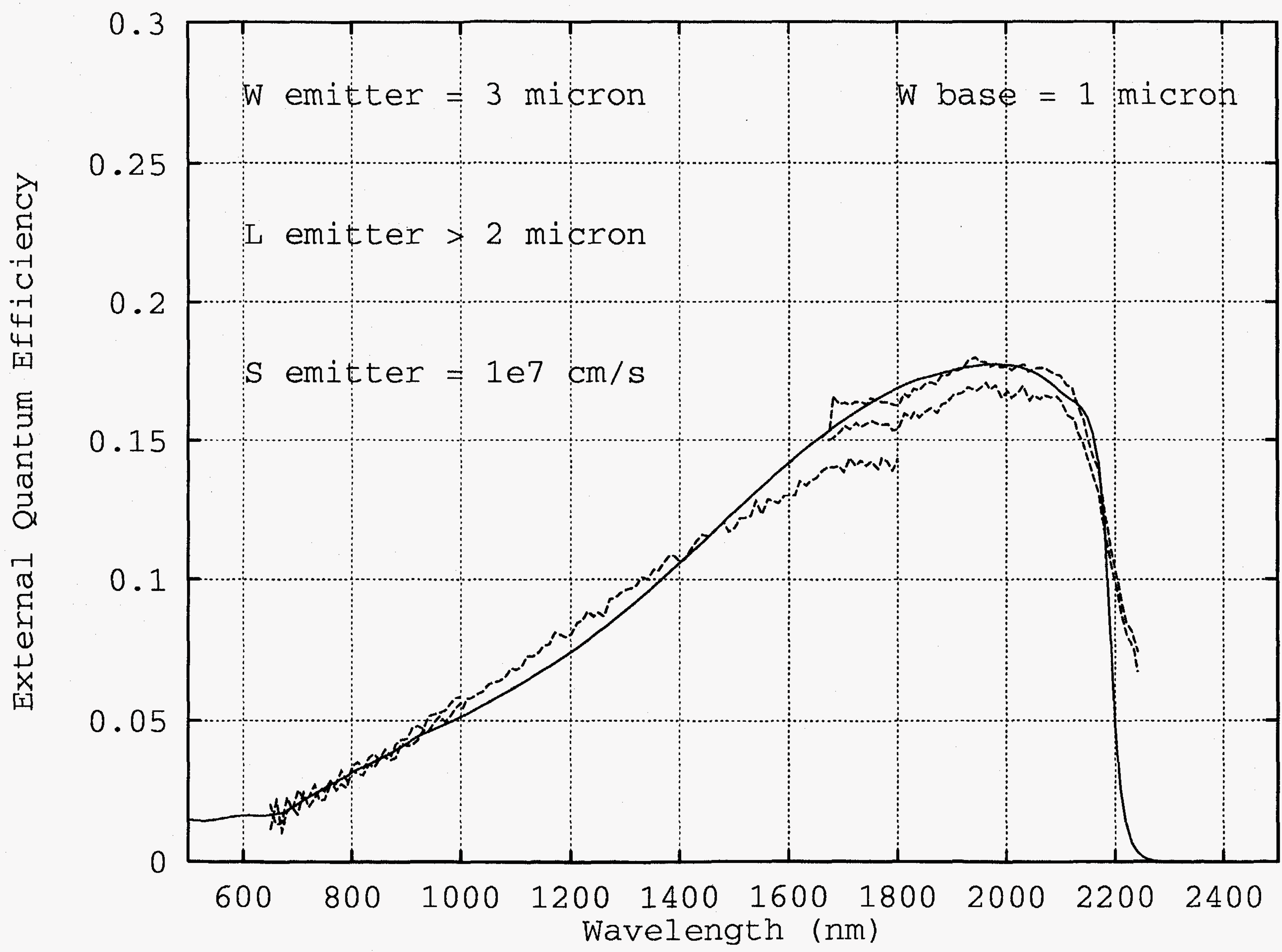

Thick P-Emitter Quaternary Device, No Passivation (device type 4)

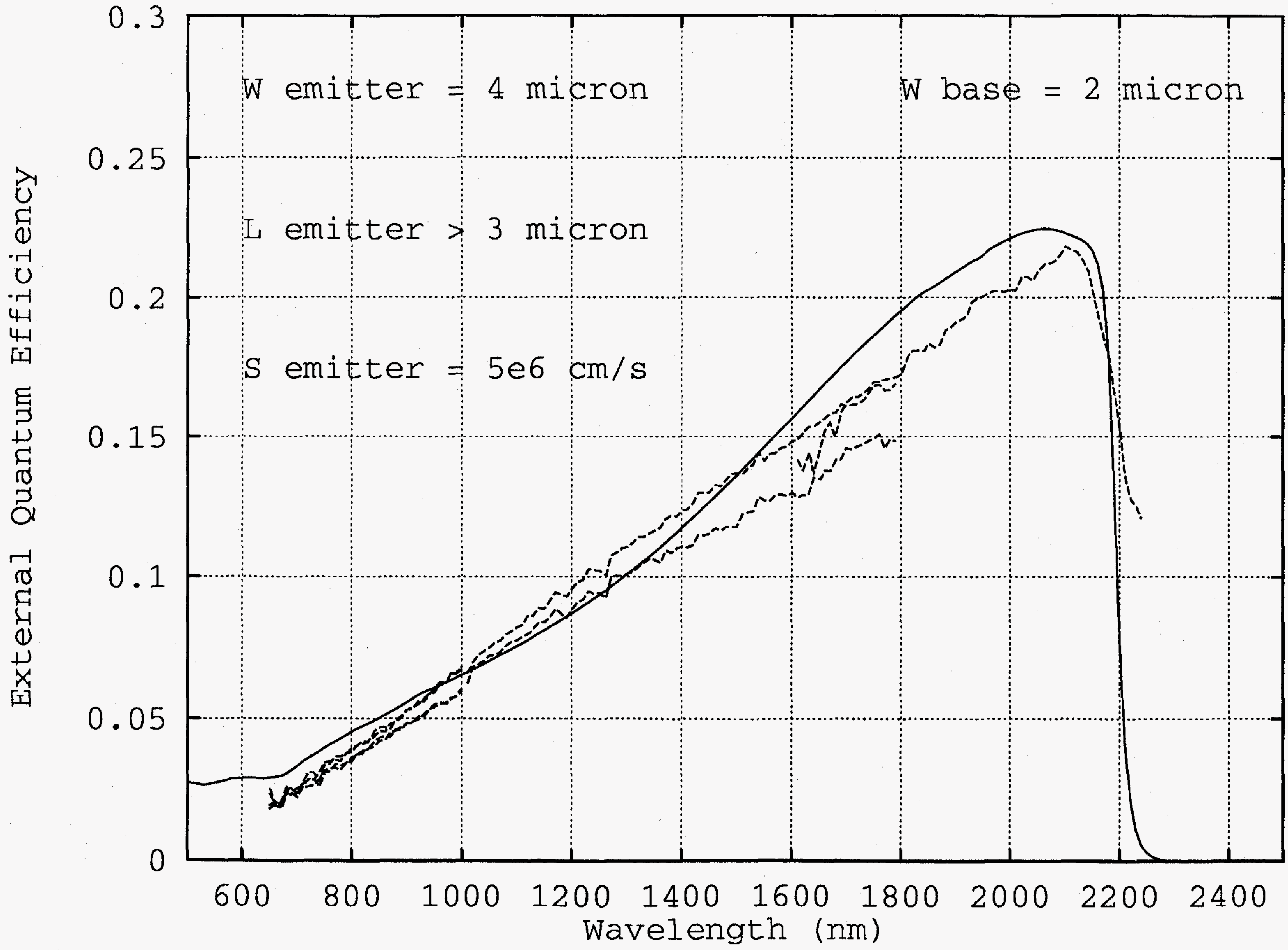

Generic TPV Device Structure

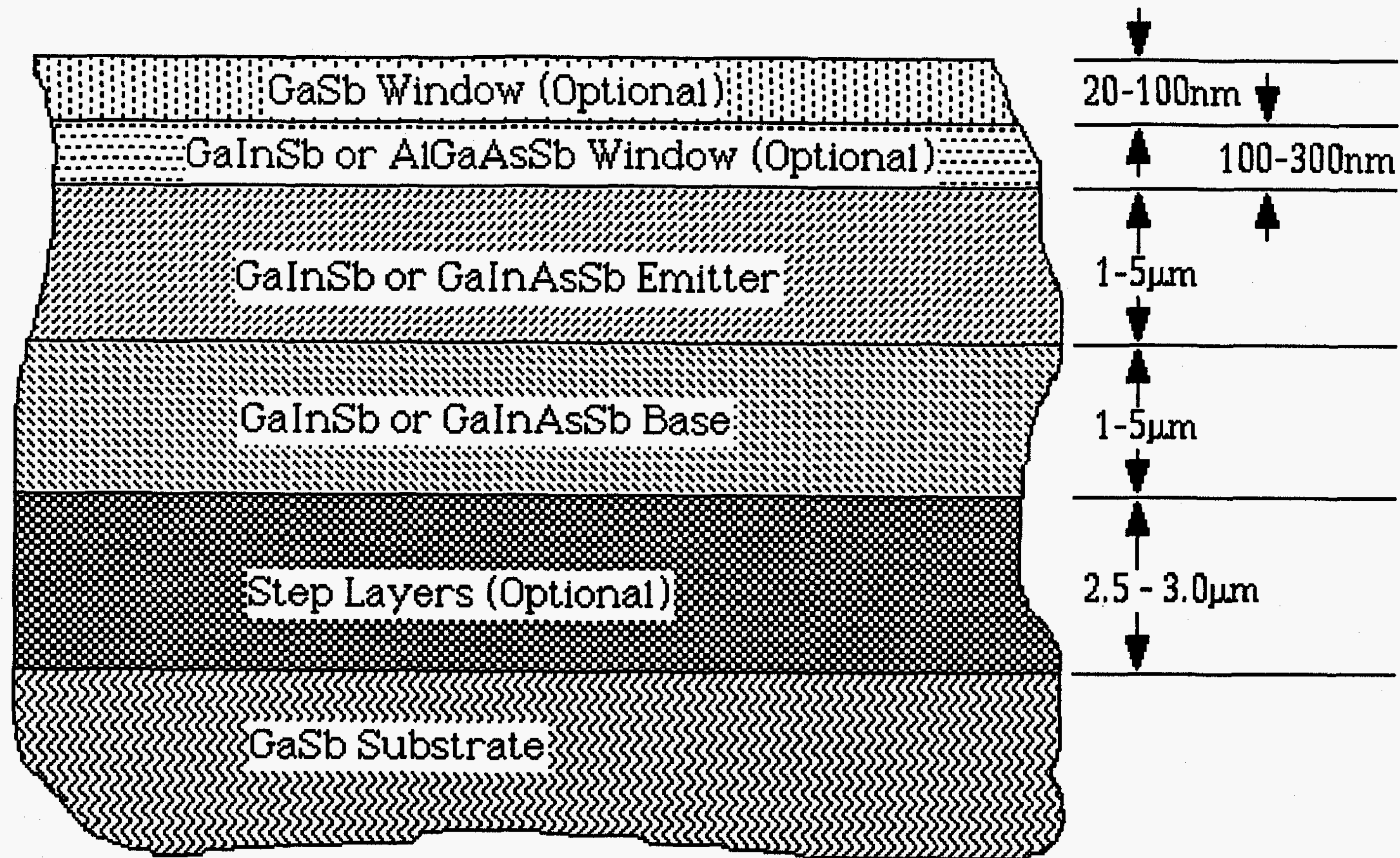

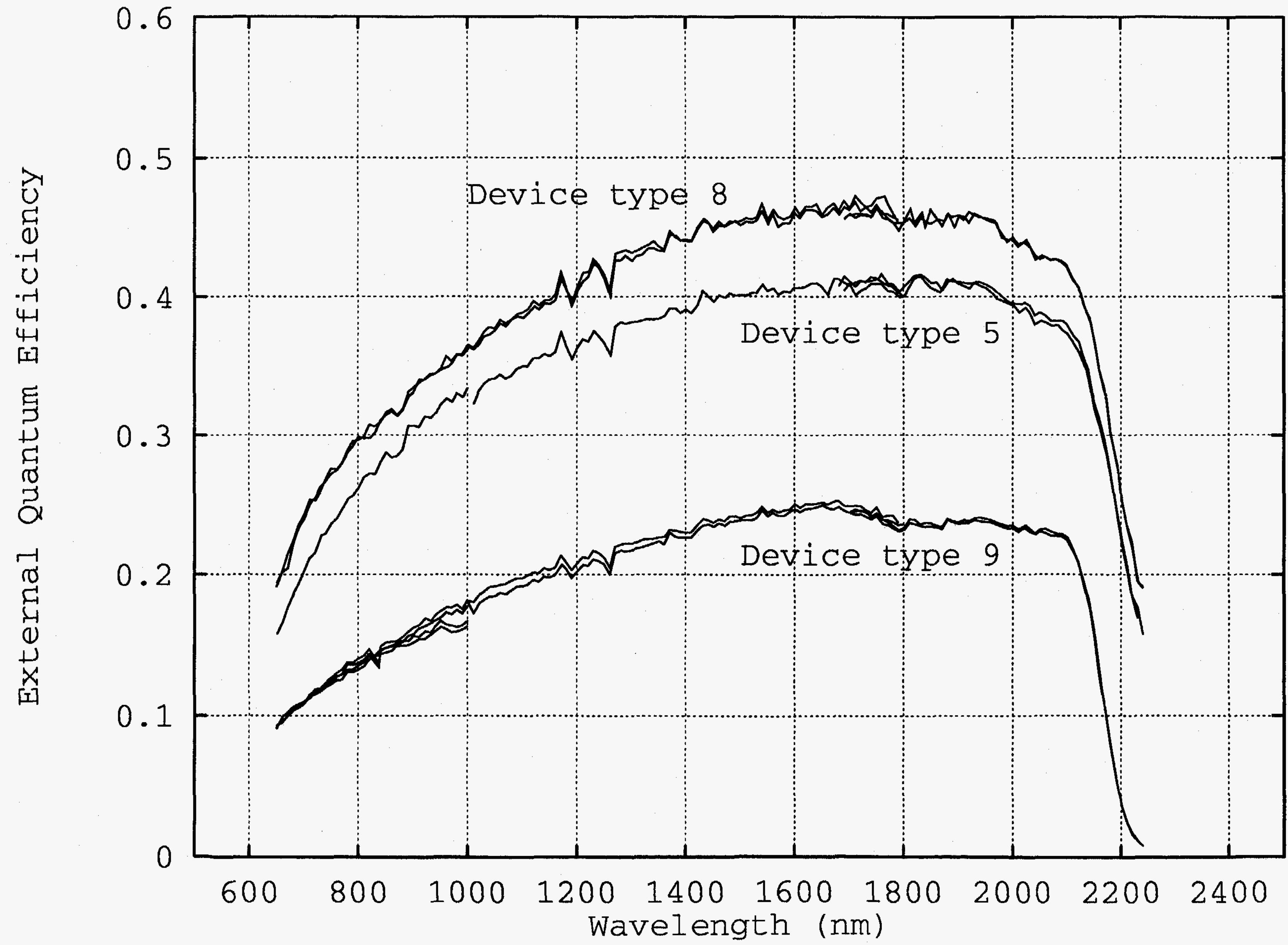
External Quantum Efficiency of Passivated Devices
External Quantum Efficiency
0.6
0.5
0.4
0.3
0.2
0.1
0
Device type 8
Device type 5
Device type 9
600
800
1000
1200
1400
1600
1800
2000
2200
2400
Wavelength (nm)

High Intensity Illumination Characteristics

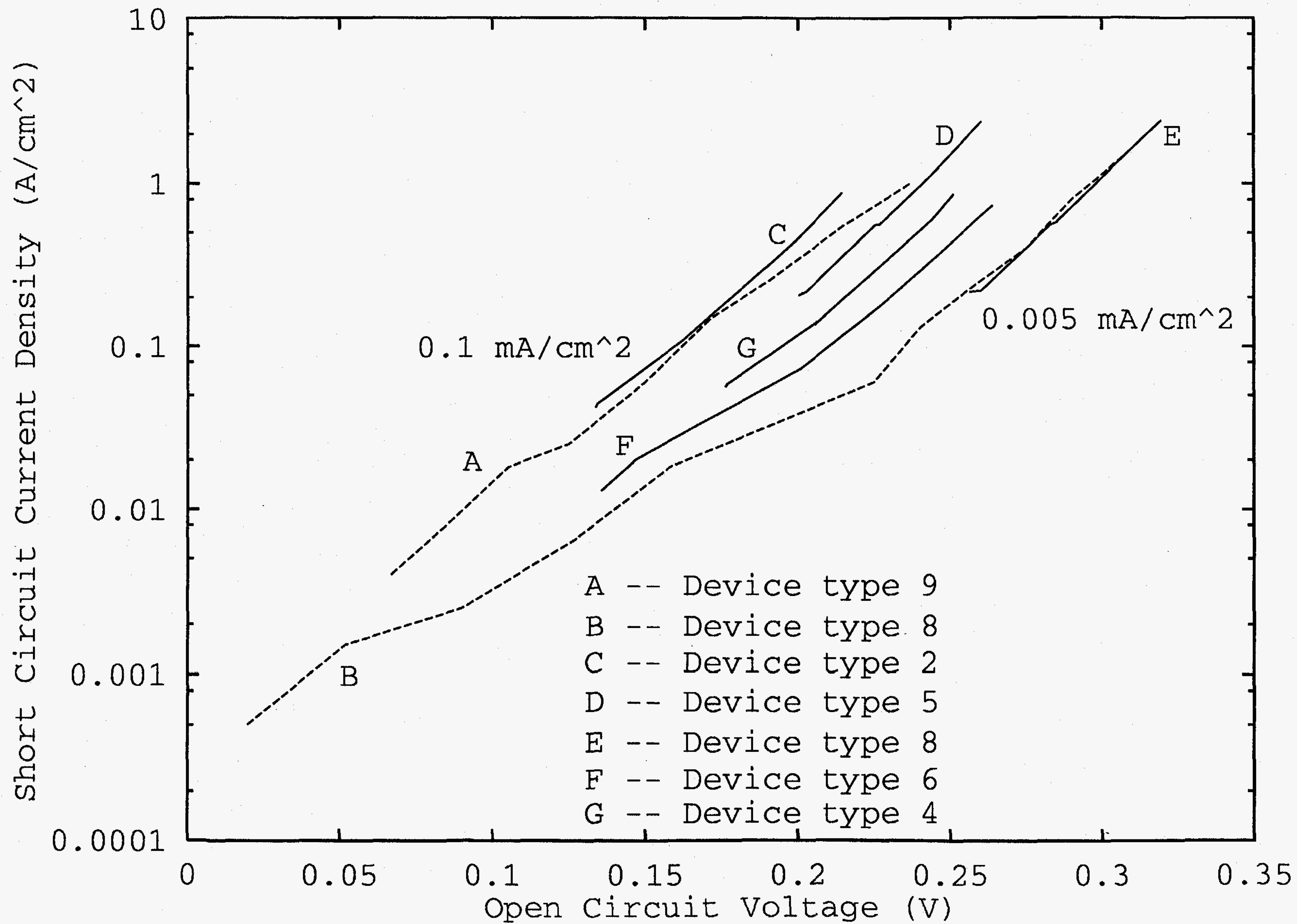

Thin P-Emitter Ternary Device, No Passivation (device type 1)

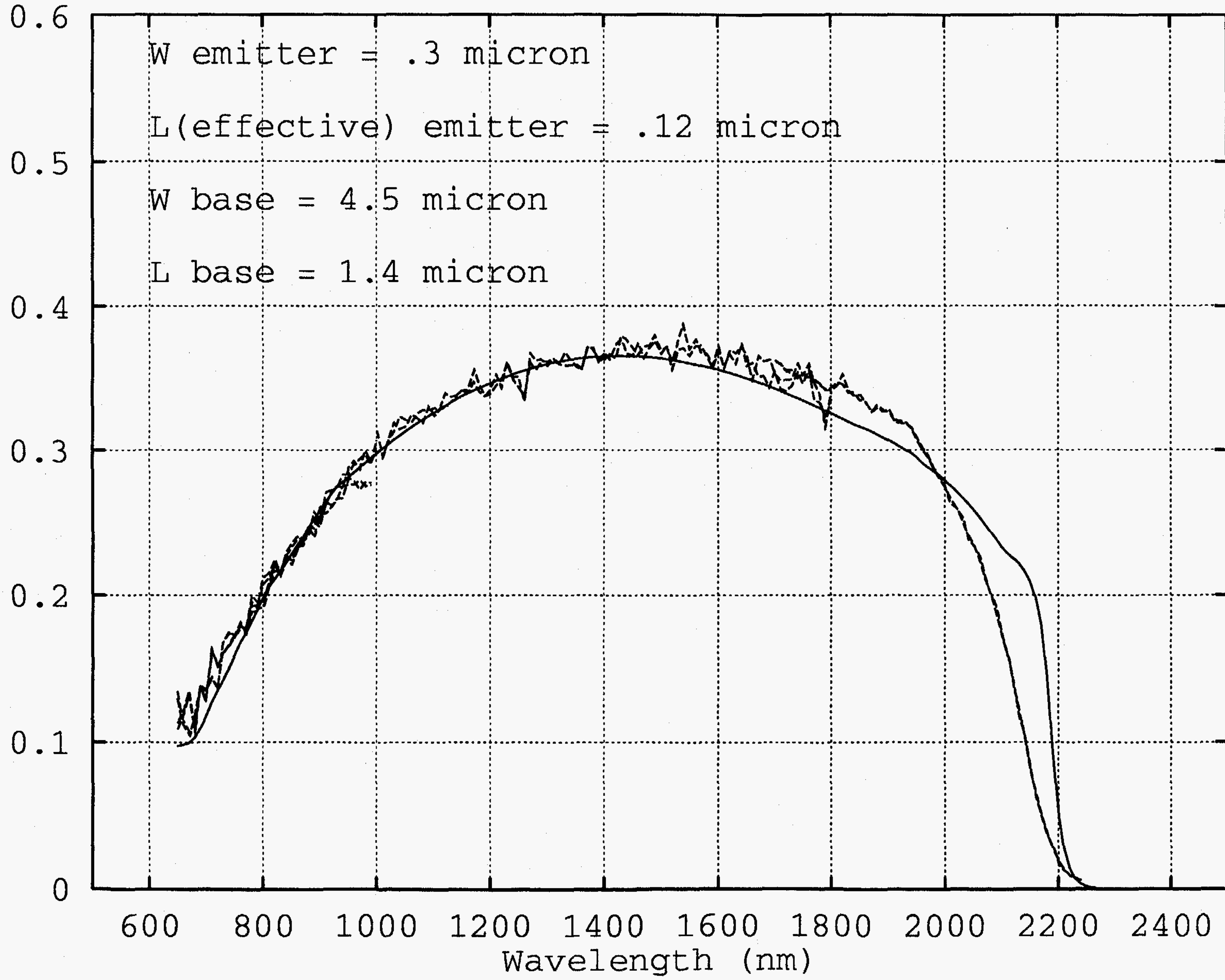

N-Emitter Device, No Passivation (device type 10)

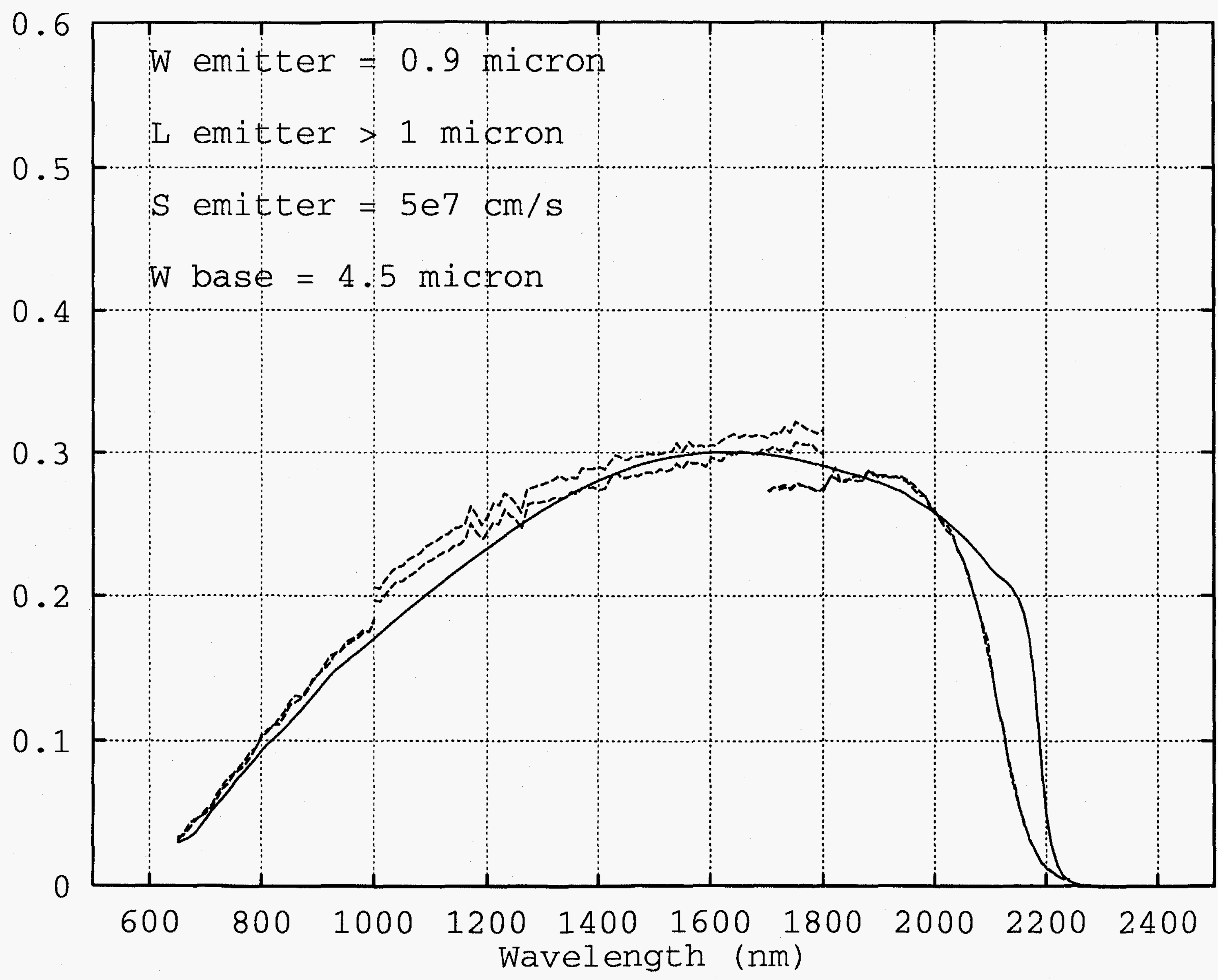

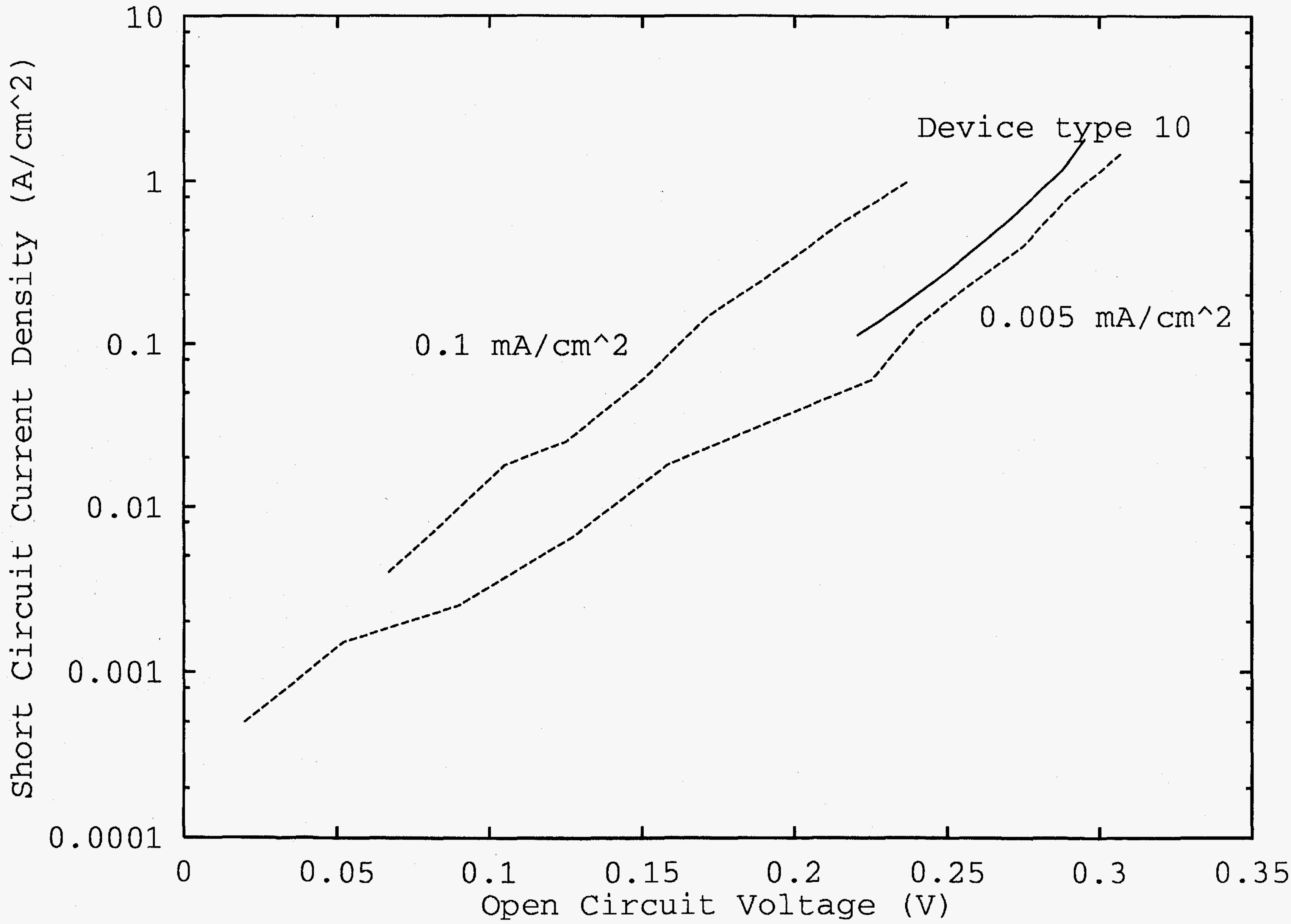
N-Emitter Device, No Passivation (device type 10)
Short Circuit Current Density (A/cm^2)
10
1
0.1
0.01
0.001
0.0001
0
0.05
0.1
0.15
0.2
0.25
0.3
0.35
Open Circuit Voltage (V)
0.1 mA/cm^2
Device type 10
0.005 mA/cm^2

Summary and Conclusions

- Optical absorption in p-layer needed for large minority carrier diffusion length;
- Thick p-emitter junctions require low surface recombination velocity for high quantum efficiency;
- Reduced dark current density necesssary for high performance TPV devices;
- Lattice-mismatched ternaries appear capable of comparable performance to lattice-matched quaternaries with comparable surface passivation;
- Thin-emitter thick-base n/p devices are promising, with high-quality shallow n-type ohmic contacts necessary.

Device Type 1

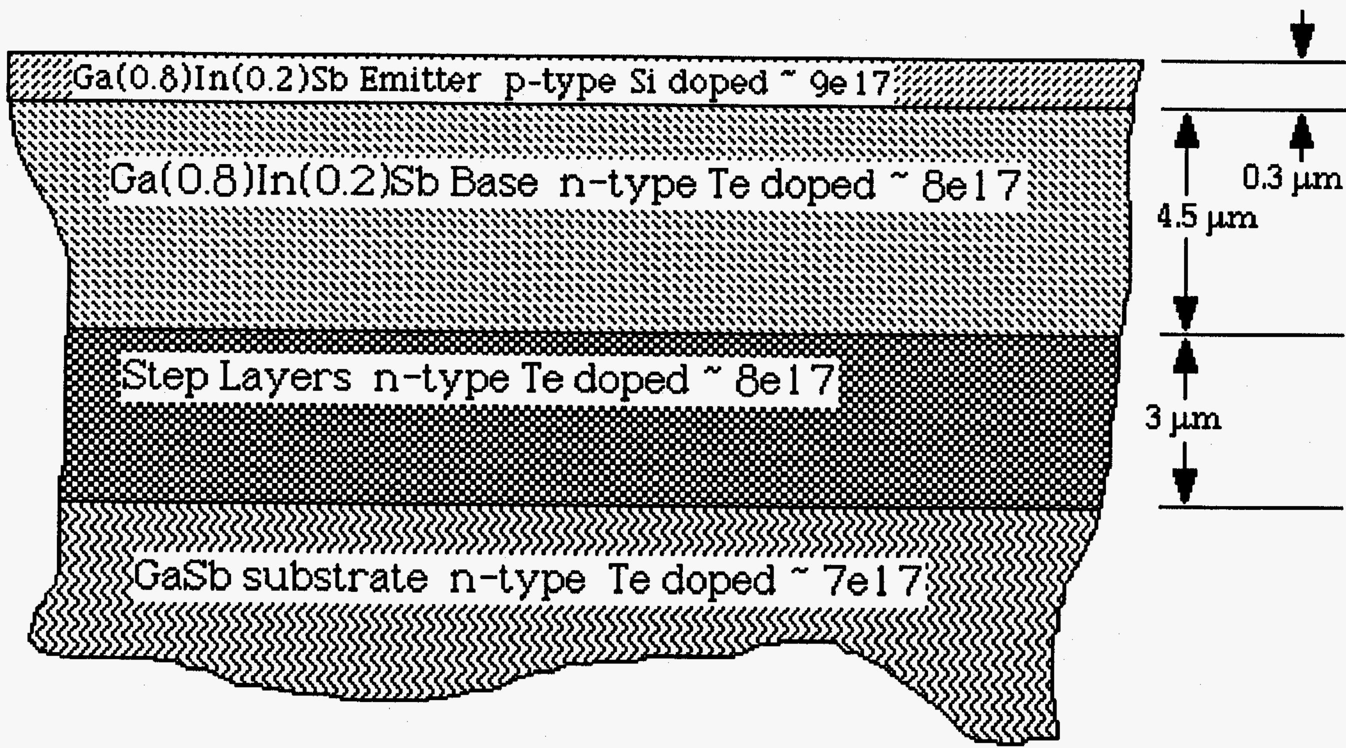

Device Type 2

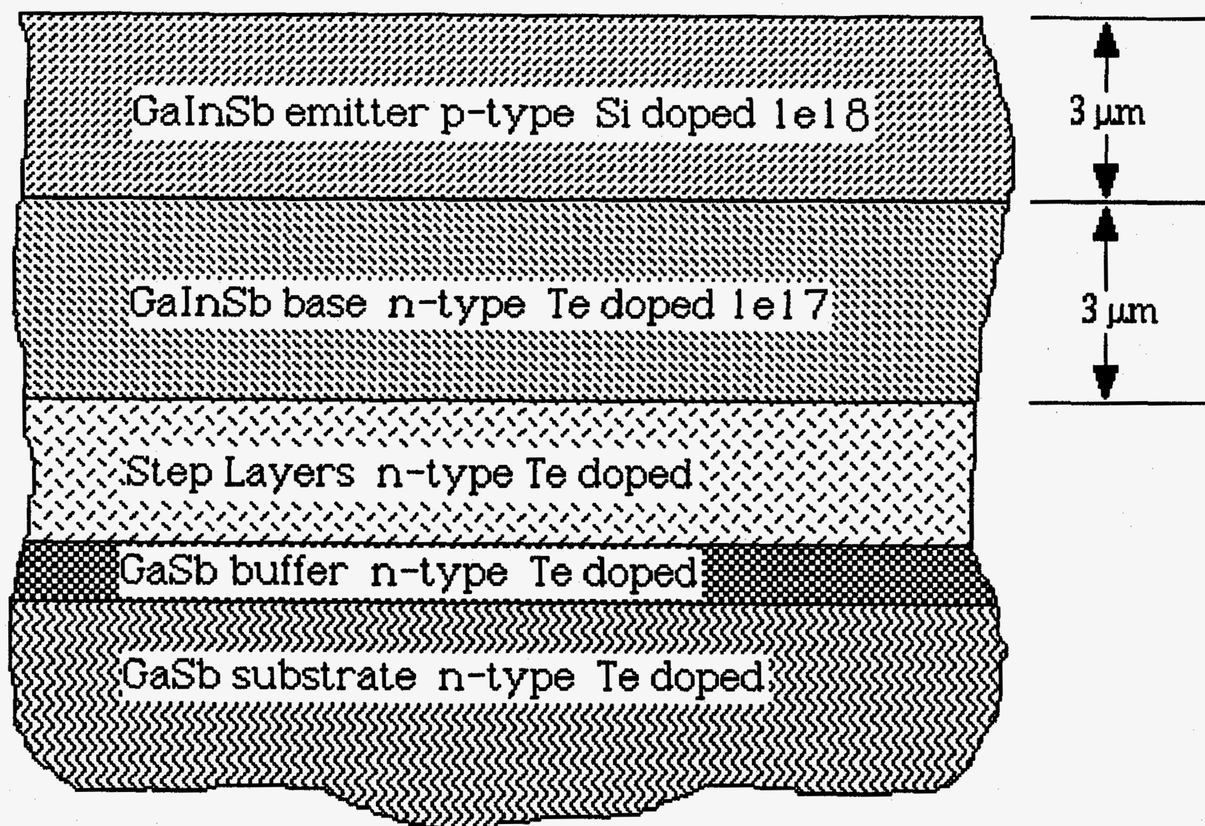

Device Type 3

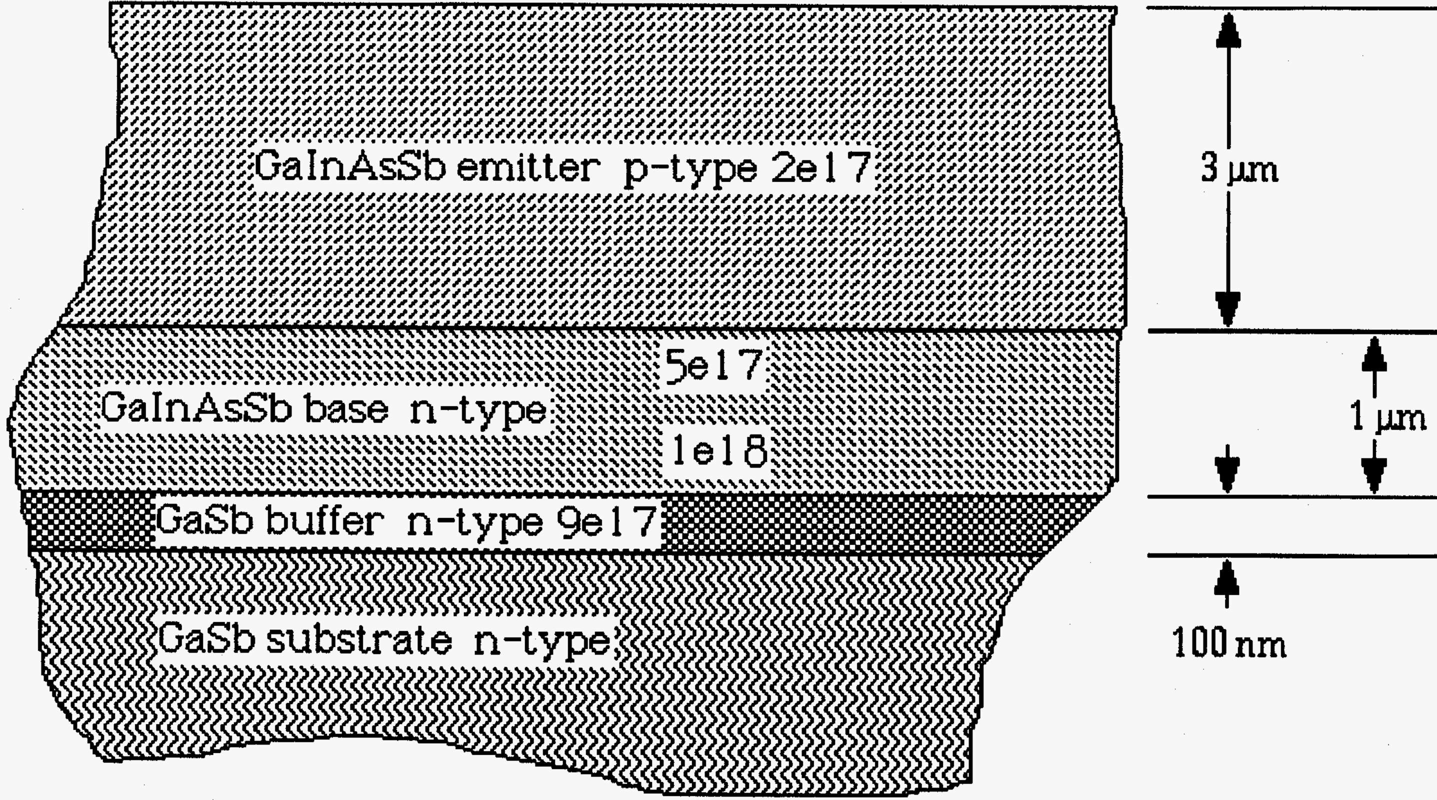

Device Type 4

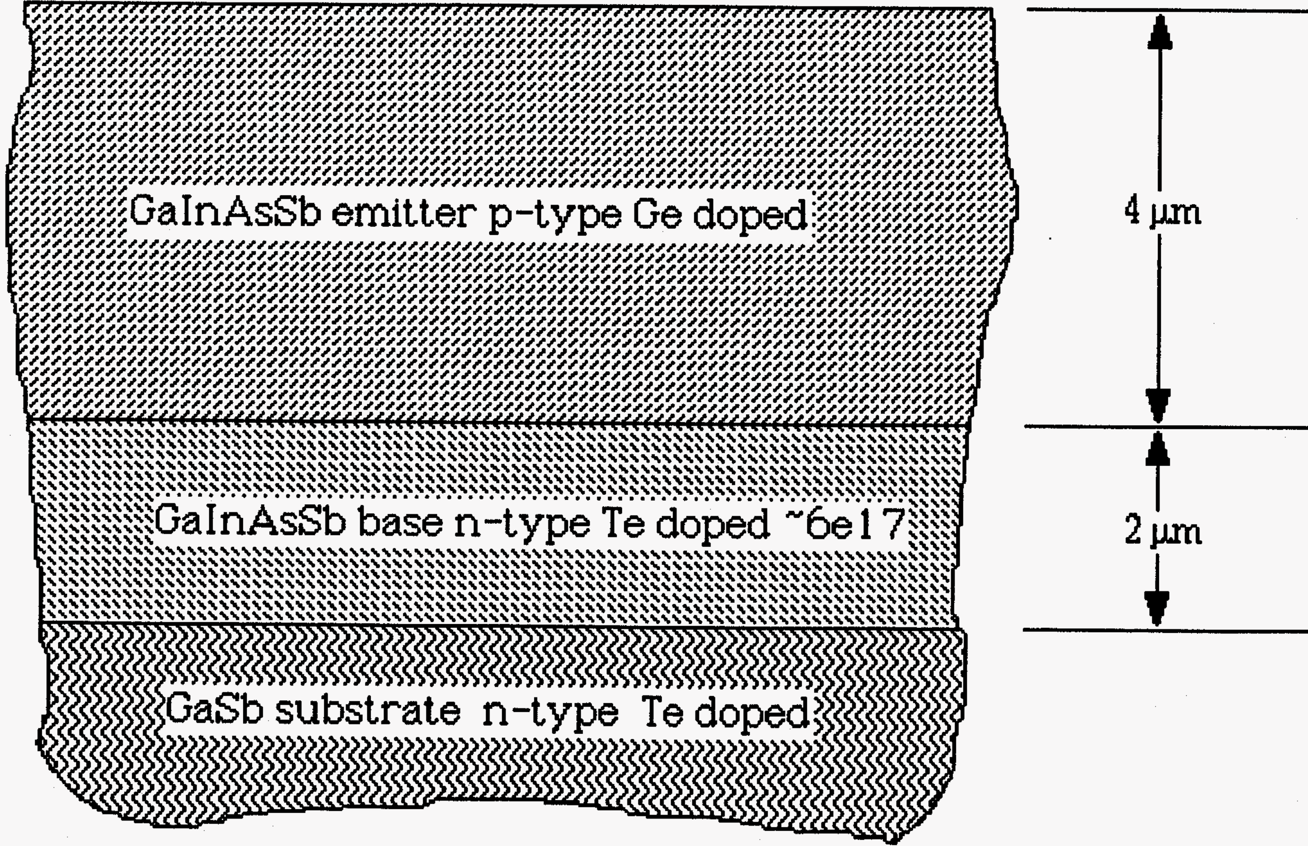

Device Type 5

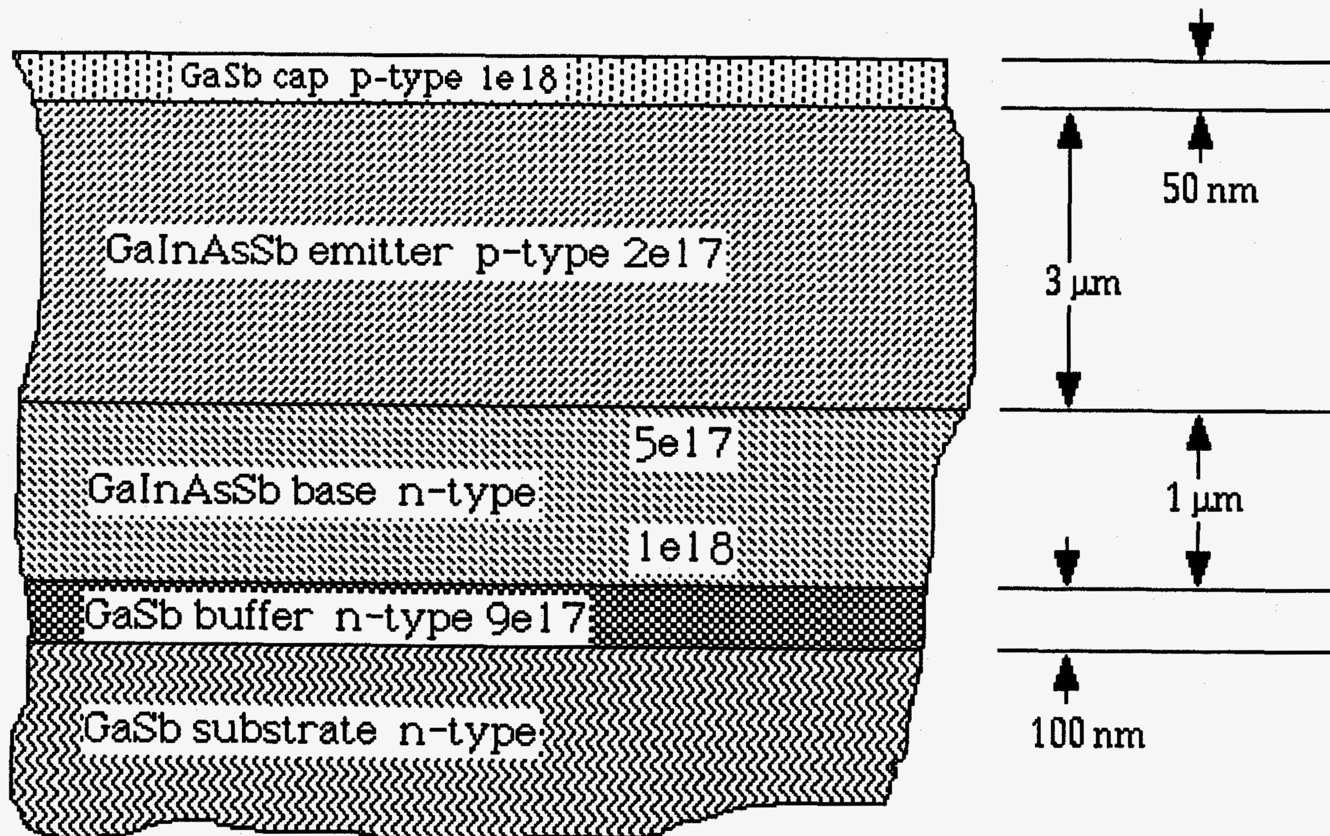

Device Type 6

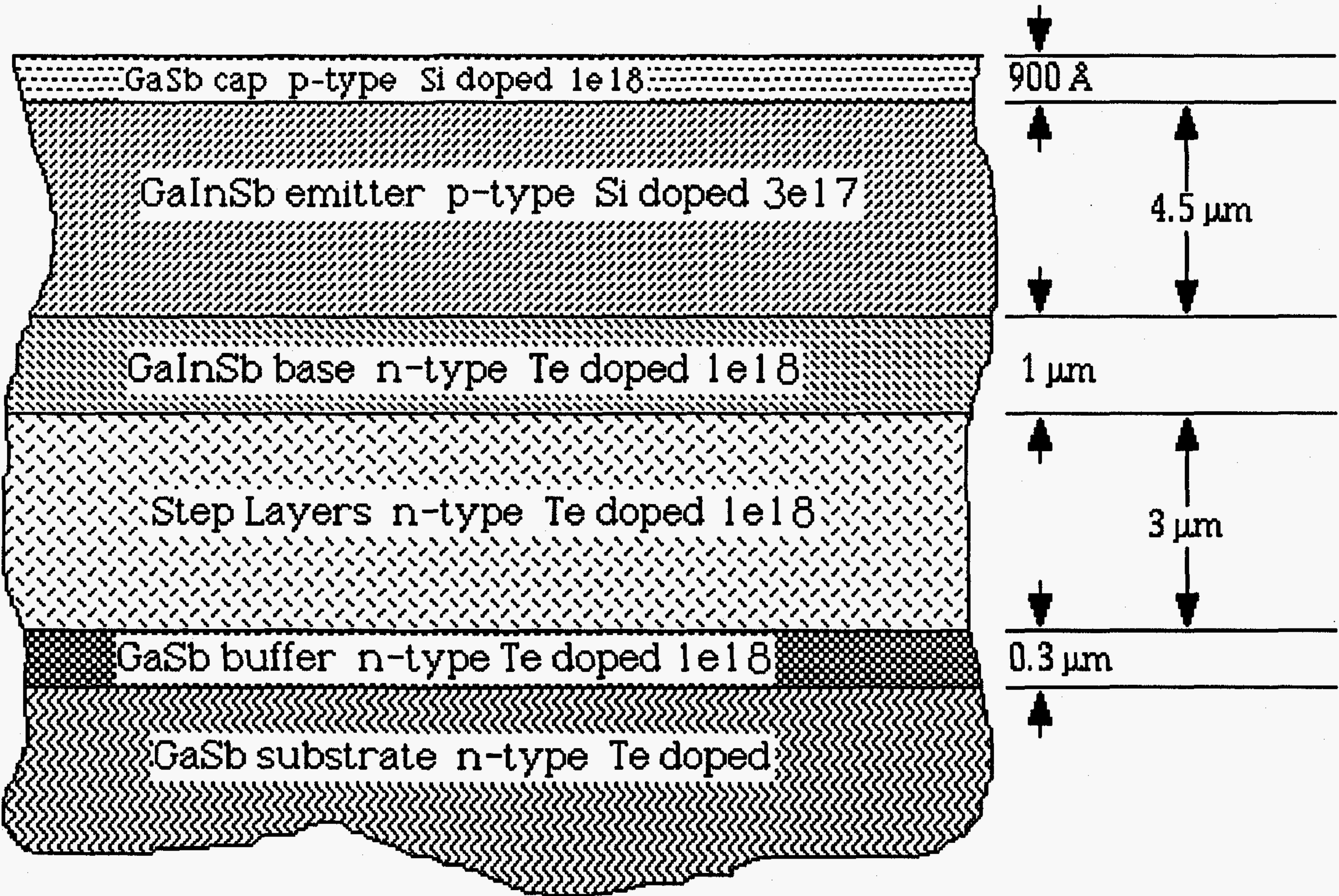

Device Type 7

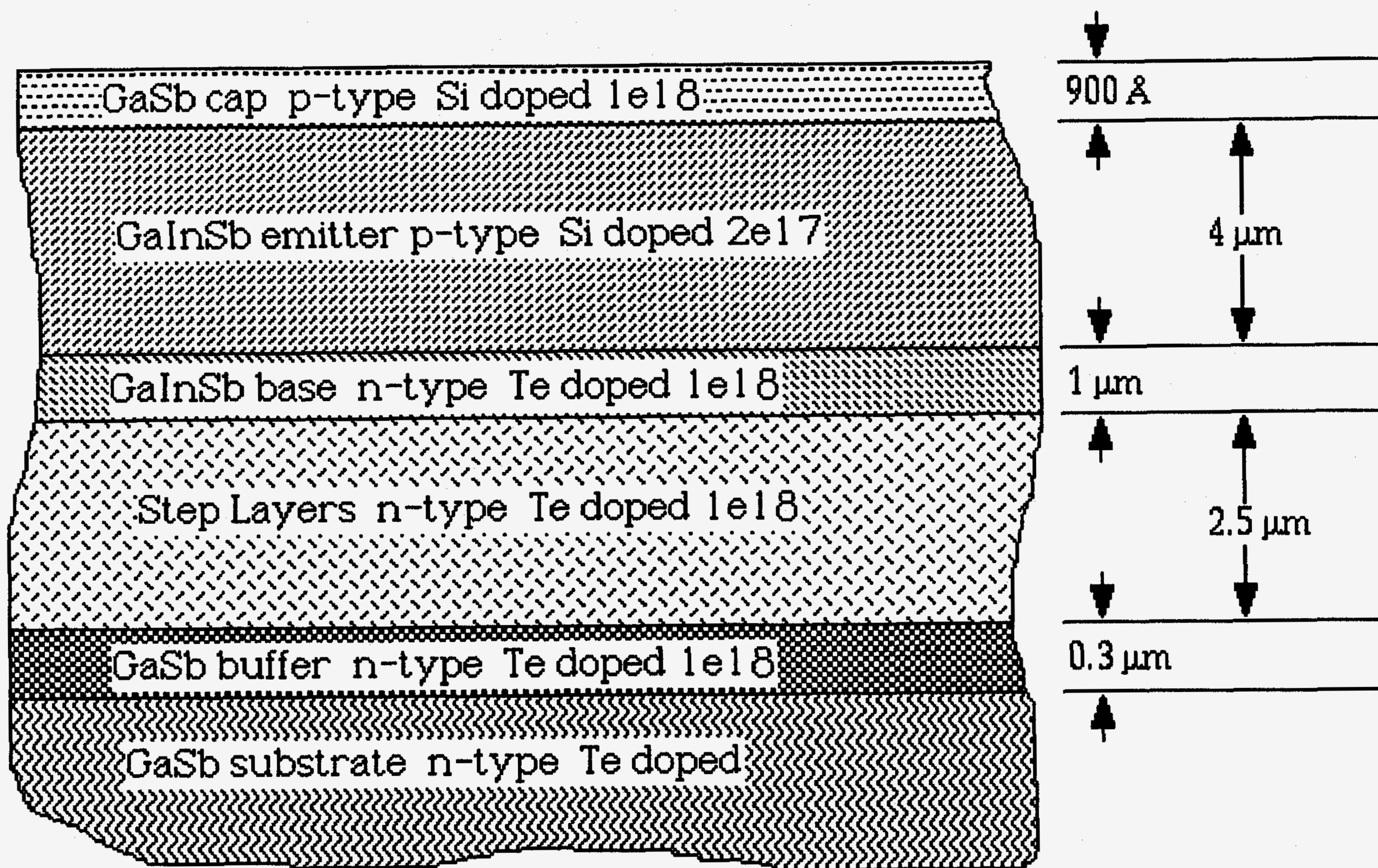

Device Type 8

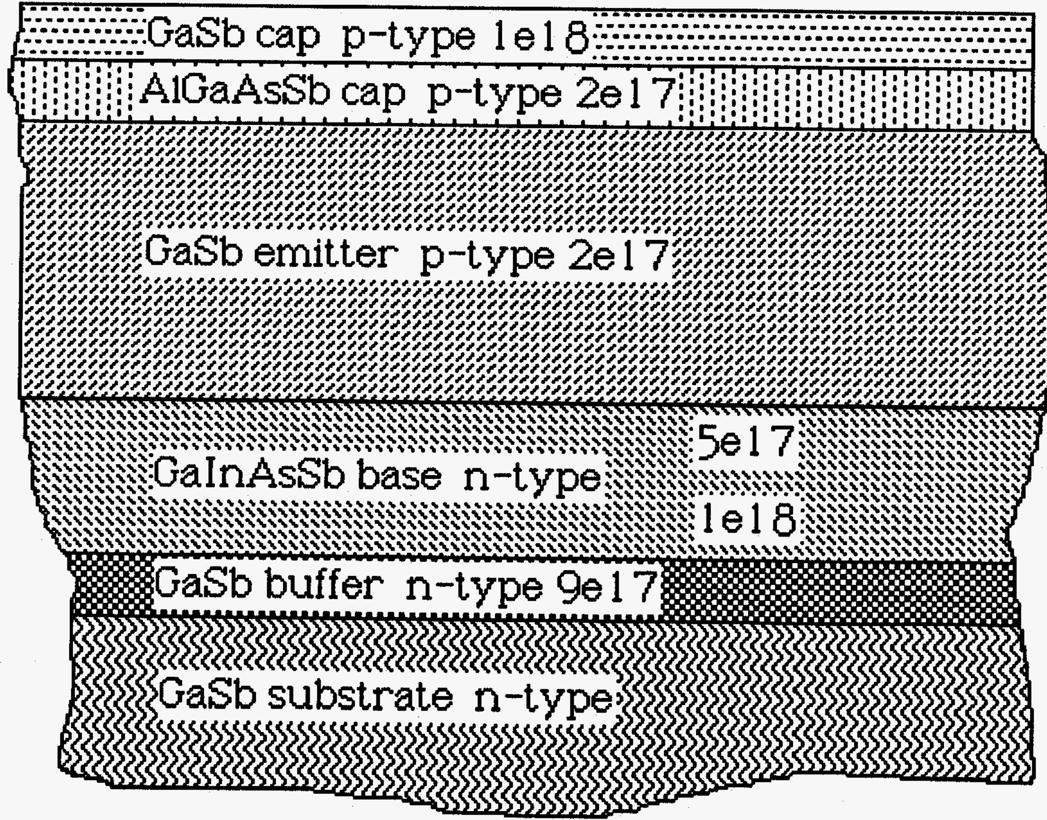

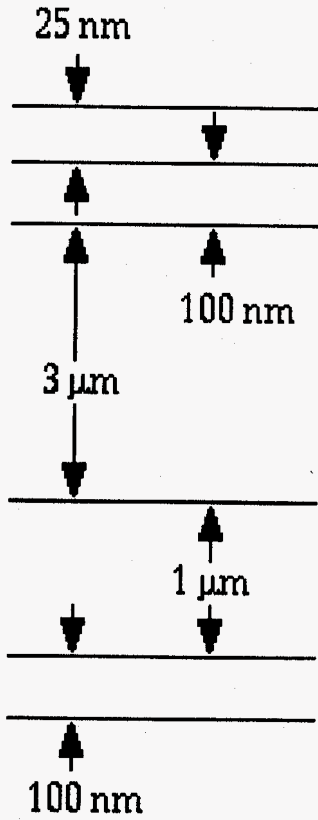

Device Type 9

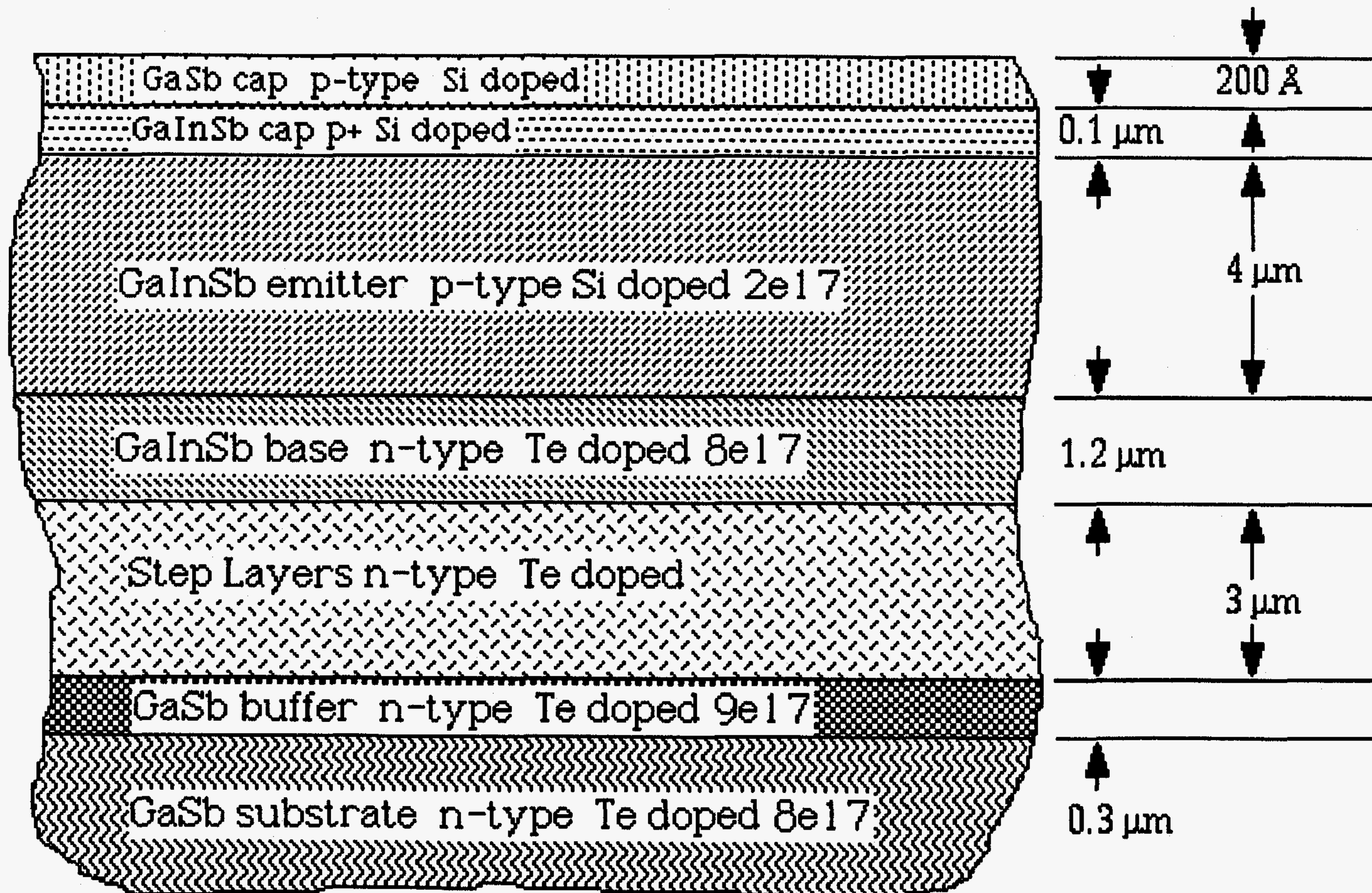

Device Type 10